

Supporting Information for:
Designing 3d Metal Oxides: Selecting Optimal Density
Functionals for Strongly Correlated Materials

Ina Østrøm,* Md. Anower Hossain,* Patrick Burr, † Judy N. Hart, ‡
Bram Hoex.*§

April 22, 2022

Contents

1 Mathematical Description of Exchange-Correlation Functionals	S2
1.1 Local Density Approximation (LDA)	S3
1.2 Generalized Gradient Approximation (GGA)	S3
1.3 Global Hybrid Functionals	S4
1.4 Range-Separated Hybrid Functionals	S5
2 Timeline of the Band Gap Problem	S5
3 Structural Parameters	S7
4 Lattice Dynamics	S13
5 Electronic Properties	S15
5.1 Band Structure and Density of States	S15
5.1.1 Magnetic Moment and Charges	S31
5.1.2 Spin Contamination	S34
5.2 Optical Properties	S35
6 Average Performances	S35
7 Input Details	S38
7.1 Geometry Input Files	S38
7.2 Basis Sets	S48

*School of Photovoltaic and Renewable Energy Engineering, University of New South Wales, Tyree Energy Technologies Building, 229 Anzac Parade, Kensington NSW 2052, Australia.

†School of Mechanical and Manufacturing Engineering, University of New South Wales, Library Rd, Kensington NSW 2052, Australia.

‡School of Materials Science & Engineering, UNSW Sydney, NSW 2052, Australia.

§Corresponding author *e-mail:* b.hoex@unsw.edu.au

1 Mathematical Description of Exchange-Correlation Functionals

The Kohn and Sham¹ formalism basis considers an fictitious system of non-interacting electrons which are subject to an external field (v_0), such that the resulting density remains identical to the exact ground-state density distribution. This allows to write a general expression for the electronic ground-state energy as a single Slater determinant (or Kohn-Sham determinant) wave function that gives the exact ground state electron density (ρ_0). The total energy functional, is given as:

$$E[\rho(r)] = K[\rho(r)] + \int v(r)\rho(r)dr + J[\rho(r)] + E_{\text{XC}}[\rho(r)] \quad (1)$$

In Equation 1, $K[\rho(r)]$ stands for kinetic energy of the non-interacting electrons, the integral for the attractive potential energy of the electron-nuclei interaction, $J[\rho(r)]$ is the Coloumbic electron-electron repulsive self interaction, and $E_{\text{XC}}[\rho(r)]$ is the exchange-correlation (XC) functional. The last energy term in Equation 1 is unknown, and so is the exchange-correlation potential:

$$v_{\text{XC}}(r) \equiv \frac{\delta E_{\text{XC}}}{\delta \rho(r)} \quad (2)$$

The $J[\rho(r)]$ term originates the self-interaction error (SIE) by considering the electron to interact with itself, and it also does not account for the correlated motion of the electrons. The electronic correlation is a dynamical effect that comes from classical Coulombic repulsion, and from the exchange repulsion of electron with the same spin (Pauli exclusion principal), which is higher in magnitude in general, and is critical to describe spin-polarized systems.² In a correlated system, as a consequence of the repulsive effects and their differences in magnitude, the electron density is not uniform, and this why the exchange-correlation term is so important. Moreover, the $E_{\text{XC}}[\rho(r)]$ in Equation 2 must include a kinetic energy correction for the interacting electrons.

The form of the Kohn-Sham equation that is analogous to the Fock equation, and that can be solved self-consistently, can be written as:

$$\left(-\frac{1}{2}\Delta + v_0 \right) \varphi_i = \varepsilon_i \varphi_i \quad (3)$$

For unrestricted Kohn-Sham calculations (UKS), spin polarization is introduced to differentiate the α and β electrons functions of the open-shell electronic structure. This generates two different versions of Equation 3 that are spin dependent, one for α and another for β electrons with $\rho_\alpha(r)$ and $\rho_\beta(r)$ density distributions, respectively.

The Hamiltonian operator v_0 (Equation 4) represents the main ansatz in DFT, which is to figure out the form of the exchange and correlation potential (Equation 2), and this is how the different rungs of density functionals of the Jacob's ladder were developed.³

$$v_0 = v + v_J + v_{\text{XC}} \quad (4)$$

where we can write v_{XC} as:

$$v_{\text{XC}} = v_X + v_C \quad (5)$$

Therefore, we can rewrite Equation 2 considering:

$$v_X(r) \equiv \frac{\delta E_X}{\delta \rho(r)} \quad (6)$$

and,

$$v_C(r) \equiv \frac{\delta E_C}{\delta \rho(r)} \quad (7)$$

Being that the contribution of the E_X is greater than E_C , however the form of the latter is where most density functionals differ from each other, hence from where different approximations originate.

1.1 Local Density Approximation (LDA)

The LDA approach to DFT is based on an electrically neutral homogeneous gas model, with the nuclear charge distributed uniformly and a localized electron density that satisfies the Pauli exclusion principle. The general form of LDA depends on the localized density ($\rho(r)$), and can be written as:

$$E_{XC}^{LDA}[\rho(r)] = \int \rho(r) \varepsilon_{XC}[\rho(r)] dr \quad (8)$$

where ε_{XC} is broken down into different expressions for exchange and correlation, as in Equations 6 and 7. The exchange part has analytical form from the homogeneous gas model (obtained by the Kohn-Sham determinants), and the main challenge arises in the different approximations for the correlation part. When spin configurations are considered in the form of $\rho_\alpha(r)$ and $\rho_\beta(r)$, the LDA becomes the local spin density approximation (LSDA).

$$E_{XC}^{LSDA}[\rho(r)] = \int \rho(r) \varepsilon_{XC}(\rho_\alpha, \rho_\beta) dr \quad (9)$$

The LDA is simple, and practical as it is computationally inexpensive. Its performance is acceptable for geometries and molecular vibrational frequencies. However, the limitations of the homogeneous gas model employed in the LDA leads to underestimation of the exchange, and overestimation of the correlation energies and this has serious implications to quantify binding energies, band structures, ionization potentials, and long-range interactions.^{4,5}

1.2 Generalized Gradient Approximation (GGA)

The semilocal GGA considers the density functional $E_{XC}[\rho(r)]$ to be both, local and non-local with respect to the electron density in a certain position, hence correct part of the LDA locality issues. To introduce this effect into $E_{XC}[\rho]$, the functional also depends on the gradient of $\rho(r)$:

$$E_{XC}^{GGA}[\rho(r)] = E_{XC}^{LSDA}[\rho(r)] + \int \rho(r) \varepsilon_{XC}(\rho_\alpha, \rho_\beta, \nabla \rho_\alpha, \nabla \rho_\beta) dr \quad (10)$$

The most popular GGA functionals are the well known PBE and BLYP, albeit B3PW, BP86, and the revised version of PBE for solids (e.g. PBESOL) are also well established functionals. The meta-GGA (mGGA) functionals, such as M06-L descends naturally from the GGA family of functionals, including an extra second derivative term $\nabla^2 \rho(r)$ from the electrons kinetic energy ($\tau(r)$) into Equation 10.⁶ Hence, the general format of mGGA XC functional is:

$$E_{XC}^{mGGA}[\rho(r)] = E_{XC}^{LSDA}[\rho(r)] + \int \rho(r) \varepsilon_{XC}(\rho_\alpha, \rho_\beta, \nabla \rho_\alpha, \nabla \rho_\beta, \tau_\alpha, \tau_\beta) dr \quad (11)$$

where $\tau(r)$ is the kinetic energy density for occupied KS orbitals, which are nonlocal functionals of the density $\rho(r)$:

$$\tau(r) = \frac{1}{2} \sum_i^{\text{occ}} |\nabla \varphi_i(r)|^2 \quad (12)$$

Although GGA and meta-GGA functionals improve some LDA limitations without adding extra computational demand, they still don't improve LDA total energies and still result in chemical bond energies overestimation, as well as have other restrictions that discussed in the main manuscript which are related to solids.

1.3 Global Hybrid Functionals

The rigorous mathematical formulation that justifies the format of hybrid density functionals is based on the adiabatic connection method, and its complete definition can found elsewhere.⁷ Herein, we define the global hybrid (GH) exchange–correlation functionals as nonlocal functionals of the occupied orbitals constructed as a linear combination of the Hartree–Fock (HF) exact exchange functional ($E_{\text{HF}} = a$) that replaces a fraction of the GGA exchange.⁸

$$E_{\text{XC}}^{\text{GH}}[\rho(r)] = (1 - a)E_{\text{X}}^{\text{DFA}}[\rho(r)] + aE_{\text{X}}^{\text{HF}} + E_{\text{C}}^{\text{DFA}}[\rho(r)] \quad (13)$$

While E_{X}^{HF} in Equation 13 is the exact exchange from HF theory, and is common to all hybrid functionals except in the amount (a) that is added, the exchange ($E_{\text{X}}^{\text{DFA}}$) and correlation ($E_{\text{C}}^{\text{DFA}}$) terms associated to DFA (density functional approximation), are exactly where the density functionals differ (and where the problems reside). For example, the "ingredients" for the famous B3LYP recipe are the Becke's three parameter (B3) hybrid functional determined with empirical atomization energies,⁹ and accounts for nonlocal weighting parameters b (weight of nonlocal part of the exchange) and c (weigh of nonlocal correlation):

$$E_{\text{XC}}^{\text{B3}} = E_{\text{XC}}^{\text{LSDA}} + a(E_{\text{X}}^{\text{HF}} - E_{\text{X}}^{\text{LSDA}}) + b(E_{\text{X}}^{\text{GGA}} - E_{\text{X}}^{\text{LSDA}}) + c(E_{\text{C}}^{\text{GGA}} - E_{\text{C}}^{\text{LSDA}}) \quad (14)$$

With the values for a , b and c in Equation 14 being 0.2, 0.72, and 0.81, respectively, and Becke's GGA exchange functional $E_{\text{X}}^{\text{B88}}$. Next, we add the correlation LSDA functional $E_{\text{C}}^{\text{VWN}}$,¹⁰ and the GGA correlation functional $E_{\text{C}}^{\text{LYP}}$.¹¹ Originally, to derive $E_{\text{XC}}^{\text{B3}}$ Becke employed the PW91 GGA correlation functional, developed by Perdew and Wang, which is known as B3PW.¹² Over the years, B3LYP became popular due to its great agreement with experimental data, regardless the lack of theoretical rigor in its formulation, which is not true for B3PW.

Another widely used hybrid functional is the PBE0, developed by Perdew, Burke and Ernzerhof.¹³ Differently of its GGA PBE version, the PBE0 adds $a = 0.25$ exact exchange E_{X}^{HF} to Equation 13, with both GGA (or DFA) exchange and correlation functionals as PBE. Although PBE0 was rationally developed by fitting high-level MP4 atomization energies to molecular experimental data,¹⁴ its lack of popularity in the solid state community is mainly due to the overestimation of band gap for some electronic systems.¹⁵

The revised version of the mGGA M06-L, known as M06, is a combination of Equation 11 and 15, in which the DFA functional is the mGGA, and the amount of the HF exchange a is 0.27.¹⁶

1.4 Range-Separated Hybrid Functionals

The family of the range-separated hybrid (RSH) functionals screen the interelectronic Coulomb potential in the HF exchange term with the Gauss (erf) and its complementary (erfc) error function in three different length scales: short ($E_{X,SR}^{HF}$), middle ($E_{X,MR}^{HF}$), and long range ($E_{X,LR}^{HF}$).¹⁷ This makes E_X^{HF} dependent on the distance between electron in the length scales of separation ($\omega(a_0^{-1})$). The scaling error function of E_X^{HF} has the format:

$$\frac{1}{r_{12}} = \left[\frac{\text{erfc}(\omega_{SR} r_{12})}{r_{12}} \right]_{SR} + \left[\frac{1 - \text{erfc}(\omega_{SR} r_{12}) - \text{erf}(\omega_{LR} r_{12})}{r_{12}} \right]_{MR} + \left[\frac{\text{erf}(\omega_{LR} r_{12})}{r_{12}} \right]_{LR} \quad (15)$$

Hence, in short range hybrid functionals such as HSE06 and HSESOL, ω_{SR} and ω_{LR} are both 0.11, and in middle range like HISS, ω_{SR} and ω_{LR} are 0.84 and 0.20, respectively.

The next step after screening the Coulomb operator with Equation 15 is to add the amount of E_X^{HF} with respect to the length scale that the functional belongs to. To do this, the general formula for the RSH functionals has the format:

$$E_{XC}^{RSH} = E_{XC}^{DFA} + c_{SR} (E_{X,SR}^{HF} - E_{X,SR}^{DFA}) + c_{MR} (E_{X,MR}^{HF} - E_{X,MR}^{DFA}) + c_{LR} (E_{X,LR}^{HF} - E_{X,LR}^{DFA}) \quad (16)$$

In Equation 16, the short RSH HSE06 and HSESOL receive both $c_{SR} = 0.25$, and the middle range HISS $c_{MR} = 0.60$.

2 Timeline of the Band Gap Problem

YEAR	TITLE
1983	Physical Content of the Exact Kohn-Sham Orbital Energies: Band Gaps and Derivative Discontinuities
1985	Density functional theory and the band gap problem
1986	Electron correlation in semiconductors and insulators: Band gaps and quasiparticle energies
1996	Generalized Kohn-Sham schemes and the band-gap problem
2005	Energy band gaps and lattice parameters evaluated with the Heyd-Scuseria-Ernzerhof screened hybrid functional
2006	Density functionals from many-body perturbation theory: the band gap for semiconductors and insulators
2007	Band gap calculations with Becke-Johnson exchange potential
2008	Localization and Delocalization Errors in Density Functional Theory and Implications for Band-Gap Prediction Accurate solid-state band gaps via screened hybrid electronic structure calculations
2009	Calculation of semiconductor band gaps with the M06-L density functional Accurate band gaps of semiconductors and insulators with a semilocal exchange-correlation potential
2011	Accurate Band Gaps for Semiconductors from Density Functional Theory Communication: A new hybrid exchange correlation functional for band-gap calculations using a short-range Gaussian attenuation
2012	Derivative discontinuity, bandgap and lowest unoccupied molecular orbital in density functional theory Challenges for Density Functional Theory On choosing the best density functional approximation Improved semiconductor lattice parameters and band gaps from a middle-range screened hybrid exchange functional
2013	Density Functional Theory and Beyond for Band-Gap Screening: Performance for Transition-Metal Oxides and Dichalcogenides Accurate screened exchange band structures for the transition metal monoxides MnO, FeO, CoO and NiO
2014	Electronic bands and excited states of III-V semiconductor polytypes with screened-exchange density functional calculations Understanding density functional theory (DFT) and completing it in practice Density functional theory in the solid state
2015	Comparing LDA-1/2, HSE03, HSE06 and GW06 approaches for band gap calculations of alloys Exchange-correlation potentials with proper discontinuities for physically meaningful Kohn-Sham eigenvalues and band structures Systematic approach for simultaneously correcting the band-gap and p-d separation errors of common cation III-V or II-VI binaries in DFT calculations within a LDA
2016	General approach for band gap calculation of semiconductors and insulators Resolution of the Band Gap Prediction Problem for Materials Design Rungs 1 to 4 of DFT Jacob's ladder: Extensive test on the lattice constant, bulk modulus, and cohesive energy of solids Predicting Band Gaps with Hybrid Density Functionals Perspective: Kohn-Sham density functional theory descending a staircase
2017	An Empirical, yet Practical Way To Predict the Band Gap in Solids by Using Density Functional Band Structure Calculations Importance of the Kinetic Energy Density for Band Gap Calculations in Solids with Density Functional Theory HLE17: An Improved Local Exchange-Correlation Functional for Computing Semiconductor Band Gaps and Molecular Excitation Energies Systematic study of the effect of HSE functional internal parameters on the electronic structure and band gap of a representative set of metal oxides Understanding band gaps of solids in generalized Kohn-Sham theory
2018	Inverse Band Structure Design via Materials Database Screening: Application to Square Planar Thermoelectrics
2019	Simple correction to bandgap problems in IV and III-V semiconductors: an improved, local first-principles density functional theory On the calculation of the bandgap of periodic solids with MGGA functionals using the total energy Laplacian free and asymptotic corrected semilocal exchange potential applied to the band gap of solids Accurate Band Gap Predictions of Semiconductors in the Framework of the Similarity Transformed Equation of Motion Coupled Cluster Theory Semilocal exchange-correlation potentials for solid-state calculations: Current status and future directions Efficient band gap prediction of semiconductors and insulators from a semilocal exchange-correlation functional Assessing model-dielectric-dependent hybrid functionals on the antiferromagnetic transition-metal monoxides MnO, FeO, CoO, and NiO Band Gap of 3D Metal Oxides and Quasi-2D Materials from Hybrid Density Functional Theory: Are Dielectric-Dependent Functionals Superior?
2020	Wannier-Koopmans method calculations for transition metal oxide band gaps A band-gap database for semiconducting inorganic materials calculated with hybrid functional Exchange-correlation functionals for band gaps of solids: benchmark, reparametrization and machine learning Tuplewise Material Representation Based Machine Learning for Accurate Band Gap Prediction
2021	Solving the strong-correlation problem in materials Efficient Band Structure Calculation of Two-Dimensional Materials from Semilocal Density Functionals Opening band gaps of low-dimensional materials at the meta-GGA level of density functional approximations Band gaps of crystalline solids from Wannier-localization-based optimal tuning of a screened range-separated hybrid functional Density functional approach to the band gaps of finite and periodic two-dimensional systems Graph network based deep learning of bandgaps Effectively improving the accuracy of PBE functional in calculating the solid band gap via machine learning The utility of composition-based machine learning models for band gap prediction Exact exchange-correlation potentials for calculating the fundamental gap with a fixed number of electrons
2022	Accurate prediction of band gap of materials using stacking machine learning model Size effect of band gap in semiconductor nanocrystals and nanostructures from density functional theory within HSE06

Figure S1: Timeline of publications discussing the DFT band gap problem for periodic systems.

3 Structural Parameters

The refcodes and references for the crystallographic structures obtained from the Inorganic Crystal Structure Database (ICSD) are: CoO (245323),¹⁸ Cr₂O₃ (75577),¹⁹ CuO (69757),²⁰ Fe₂O₃ (173651),²¹ MnO (9864),²² NiO (9866),²² V₂O₃ (1869),²³ Cu₂O (52043),²⁴ TiO₂ (23697),²⁵ V₂O₅ (43132),²⁶ and ZnO (290322).²⁷ Crystal structures and details are shown in Figures S2, S3 and S4.

Crystallographic Cell Structure			
IUPAC Name			
Titanium(IV) oxide	Vanadium(III) oxide	Vanadium(V) oxide	Chromium(III) oxide
Mineral Name			
Rutile	Karelianite	Shcherbinaite	Eskolaite
Chemical Formula			
TiO ₂	V ₂ O ₃	α -V ₂ O ₅	Cr ₂ O ₃
Space Group			
P42/mnm (136)	R-3cH (167)	PmmnZ (59)	R-3cH (167)
Crystal System			
Tetragonal	Trigonal	Orthorhombic	Trigonal
Structure Type			
-	Corundum	-	Corundum
Cell Parameters (a b c α β γ)			
4.5937 4.5937 2.9587 90.000 90.000 90.000	4.9492 4.9492 13.9980 90.000 90.000 120.000	3.5710 11.5440 4.3830 90.000 90.000 90.000	4.9570 4.9570 13.5923 90.000 90.000 120.000

Figure S2: Crystallographic unit structures of TiO₂, V₂O₃, V₂O₅ and Cr₂O₃. Color-code: *light blue* = titanium, *pink* = vanadium, *dark blue* = chromium, *red* = oxygen.

Crystallographic Cell Structure			
IUPAC Name			
Manganese(II) oxide	Iron(III) oxide	Cobalt(II) oxide	Nickel(II) oxide
Mineral Name			
Manganosite	Hematite	-	Bunsenite
Chemical Formula			
MnO	$\alpha\text{-Fe}_2\text{O}_3$	CoO	NiO
Space Group			
Fm-3m (225)	R-3cH (167)	Fm-3m (225)	Fm-3m (225)
Crystal System			
Cubic	Trigonal	Cubic	Cubic
Structure Type			
Rock salt	Corundum	Rock salt	Rock salt
Cell Parameters (a b c α β γ)			
4.4460 4.4460 4.4460 90.000 90.000 90.000	5.0346 5.0346 13.7533 90.000 90.000 120.000	4.2600 4.2600 4.2600 90.000 90.000 90.000	4.1780 4.1780 4.1780 90.000 90.000 90.000

Figure S3: Crystallographic unit cell structures of MnO, Fe_2O_3 , CoO and NiO. Color-code: green = manganese, dark orange = iron, gold = cobalt, light grey = nickel, red = oxygen.

Crystallographic Cell Structure		
IUPAC Name		
Copper(II) oxide	Copper(I) oxide	Zinc(II) oxide
Mineral Name		
Tenorite	Cuprite	Zincite
Chemical Formula		
CuO	Cu ₂ O	ZnO
Space Group		
C1/c1 (9)	Pn-3mZ (224)	P3 (143)
Crystal System		
Monoclinic	Cubic	Trigonal
Structure Type		
-	-	Wurtzite
Cell Parameters (a b c α β γ)		
4.6927 3.4283 5.1370 90.000 99.546 90.000	4.2685 4.2685 4.2685 90.000 90.000 90.000	3.2468 3.2468 5.2019 90.000 90.000 120.000

Figure S4: Crystallographic unit cell structures of CuO, Cu₂O, and ZnO. Color-code: *light pink* = copper, *dark grey* = zinc, *red* = oxygen.

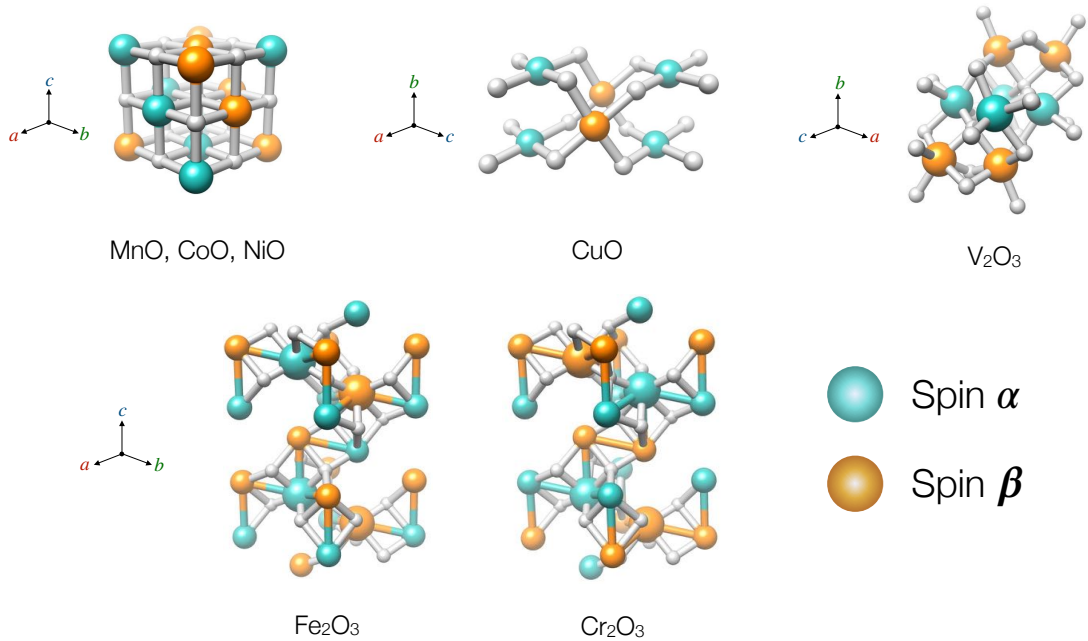


Figure S5: Spin ordering for antiferromagnetic (AFII) open-shell insulators.

	E _{HF} (%)	0.00	0.00	0.00	0.00	20.00	20.00	20.00	25.00	25.00	25.00	25.00	27.00	33.33	60.00
TMOs	ρ_{bulk}	PBE	BLYP	PBESOL	M06L	B3PW	B3PBE	B3LYP	PBE0	PBESOL0	HSE06	HSESOL	M06	PBE0-13	HISS
CoO	6.43	6.69	6.21	7.06	6.47	6.40	6.50	6.23	6.42	6.66	6.43	6.66	6.51	6.44	6.49
CuO	6.34	5.75	5.52	6.04	6.34	6.11	6.37	5.73	6.35	6.67	6.34	6.66	5.89	6.46	6.57
Cu ₂ O	5.85	5.81	5.52	6.13	5.89	5.82	5.94	5.61	5.85	6.08	5.85	6.09	5.82	5.86	5.89
Cr ₂ O ₃	5.18	5.09	4.94	5.31	5.07	5.15	5.21	5.04	5.18	5.31	5.18	5.31	5.12	5.21	5.23
Fe ₂ O ₃	5.20	5.18	5.00	5.49	5.14	5.17	5.23	5.05	5.20	5.36	5.20	5.33	5.17	5.24	5.27
MnO	5.39	5.39	5.20	5.64	5.36	5.36	5.44	5.24	5.38	5.55	5.39	5.55	5.36	5.43	5.43
NiO	6.69	6.64	6.37	7.00	6.59	6.66	6.77	6.48	6.69	6.94	6.69	6.94	6.58	6.72	6.77
V ₂ O ₅	3.34	2.85	2.68	3.04	3.14	2.95	2.91	3.01	3.11	3.25	3.13	3.24	3.23	3.14	4.12
V ₂ O ₅ *	3.34	3.13	3.21	3.29	3.18	3.73	3.75	3.60	3.58	3.66	3.62	3.67	3.34	3.62	N/A
V ₂ O ₃	4.90	4.98	4.81	5.21	4.92	4.88	4.94	4.77	4.89	5.02	4.90	5.03	4.84	4.91	4.92
ZnO	5.51	5.36	5.19	5.60	5.45	5.48	5.56	5.36	5.52	5.68	5.51	5.68	5.55	5.56	5.61
TiO ₂	4.32	4.18	4.07	4.31	4.23	4.29	4.33	4.21	4.32	4.41	4.32	4.41	4.28	4.36	4.38

Max.
Min.

Figure S6: Bulk density ρ_{bulk} (g/cm³) values calculated with different density functionals. Experimental data (first column) references: CoO,¹⁸ Cr₂O₃,¹⁹ CuO,²⁰ Fe₂O₃,²¹ MnO,²² NiO,²² V₂O₃,²³ Cu₂O,²⁴ TiO₂,²⁵ V₂O₅,²⁶ and ZnO.²⁷

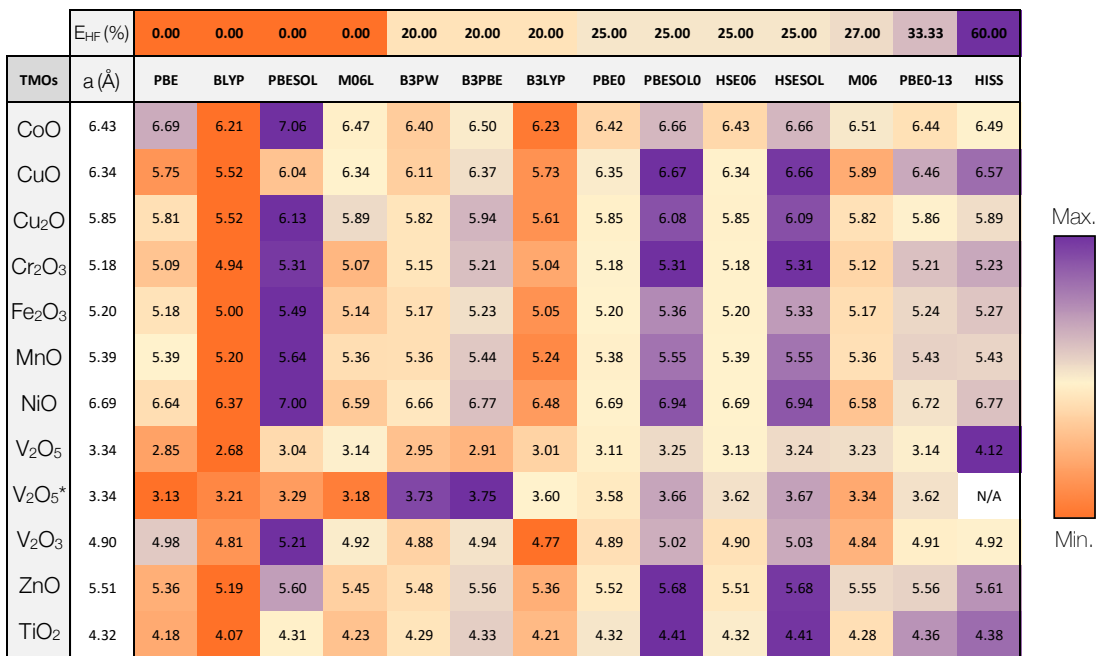


Figure S7: Lattice parameter a (\AA) values calculated with different density functionals. for V₂O₅, b is shown. Experimental data (first column) references: CoO,¹⁸ Cr₂O₃,¹⁹ CuO,²⁰ Fe₂O₃,²¹ MnO,²² NiO,²² V₂O₃,²³ Cu₂O,²⁴ TiO₂,²⁵ V₂O₅,²⁶ and ZnO.²⁷

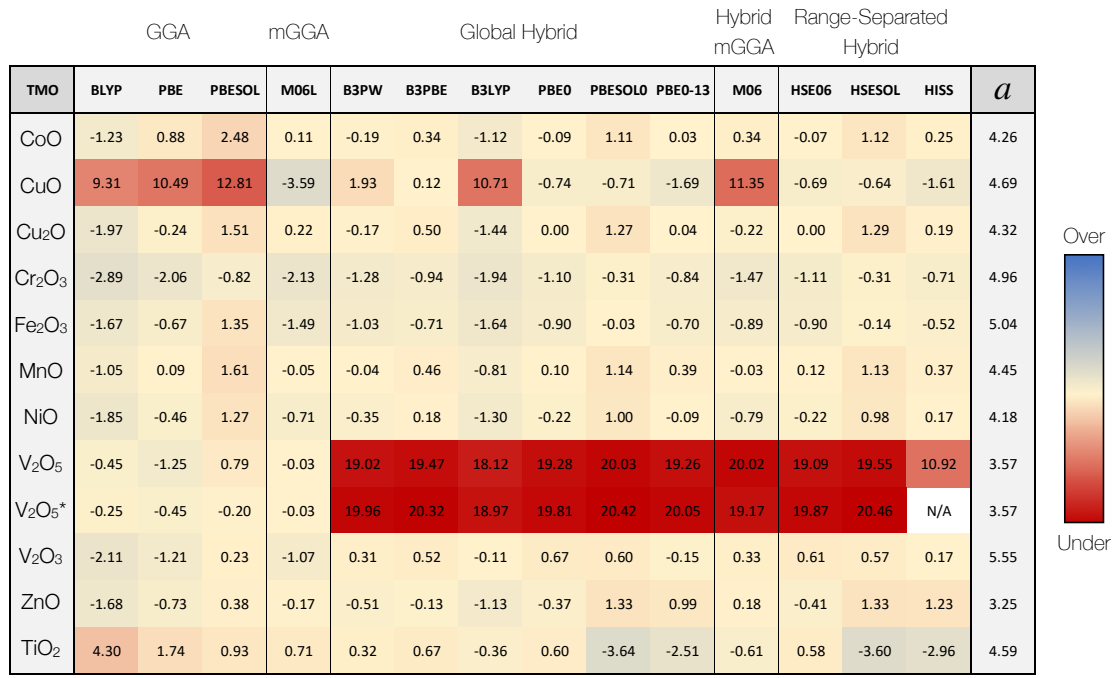


Figure S8: Colormap of the lattice parameter a relative approximation error. The layered structure V₂O₅* includes D3-BJ corrections.

4 Lattice Dynamics

Table S1: Experimental values of phonon vibrational modes, transverse and longitudinal optical (TO and LO) splitting, transverse and longitudinal acoustic (TA and LA) frequencies, and frequency wavenumbers ω_ν (cm^{-1}) that are infrared (g) and Raman (u) active for the transition metal oxides.

CuO ^{28–30}		Cu ₂ O ^{28,31,32}		ZnO ^{28,33–35}		MnO ^{36–38}		CoO ^{36,39}		NiO ^{36,40}	
Mode	ω_ν	Mode	ω_ν	Mode	ω_ν	Mode	ω_ν	Mode	ω_ν	Mode	ω_ν
A _g	296	ν_{TO} F _{1u}	146	ν_1 E _{2u}	101	ν_{LO} (Γ)	492	ν_{LO} (Γ)	523	ν_{LO} (Γ)	577
B _{1g}	344	ν_{LO} F _{1u}	149	ν_2 E _{2u}	437	ν_{TO} (Γ)	258	ν_{TO} (Γ)	350	ν_{TO} (Γ)	387
B _{2g}	629	$\nu_{\text{TO,LO}}$ F _{1u}	176	ν_{TO} E _{1u}	407	ν_{TO} (X)	348	ν_{TO} (X)	415	ν_{TO} (X)	430
A _{1u}	161	F _{2g}	514	ν_{TO} A _{1u}	380	ν_{TA} (X)	161	ν_{TA} (X)	167	ν_{TA} (X)	181
A _{2u}	321	ν_{TO} F _{1u}	634	ν_{LO} E _{1u}	583						
A _{3u}	478	ν_{LO} F _{1u}	664	ν_{LO} A _{1u}	574						
B _{1u}	147			ν_{TO} E _{1g}	412						
B _{2u}	530			ν_{LO} E _{1g}	591						
B _{3u}	590			ν_{TO} A _{1g}	380						
				ν_{LO} A _{1g}	570						
TiO ₂ ⁴¹		Cr ₂ O ₃ ^{42–44}		Fe ₂ O ₃ ^{43,44}		V ₂ O ₃ ^{45,46}		V ₂ O ₅ ⁴⁷			
Mode	ω_ν	Mode	ω_ν	Mode	ω_ν	Mode	ω_ν	Mode	ω_ν	Mode	ω_ν
B _{1g}	143	$\nu_{1,\text{TO}}$ E _g	417	ν_1 A _{1g}	225	ν_1 A _{1g}	234	$\nu_{1,\text{TO}}$ B _{1u}	140	$\nu_{3,\text{TO}}$ B _{2u}	506
E _{2u}	447	$\nu_{2,\text{TO}}$ E _g	444	ν_2 A _{1g}	500	ν_2 A _{1g}	501	$\nu_{1,\text{LO}}$ B _{1u}	140	$\nu_{3,\text{LO}}$ B _{2u}	844
A _{1g}	612	$\nu_{3,\text{TO}}$ E _g	532	ν_1 E _g	246	ν_1 E _g	210	$\nu_{2,\text{TO}}$ B _{1u}	290	$\nu_{1,\text{TO}}$ B _{3u}	72
B _{2g}	826	$\nu_{4,\text{TO}}$ E _g	613	ν_2 E _g	290	ν_2 E _g	246	$\nu_{2,\text{LO}}$ B _{1u}	290	$\nu_{1,\text{LO}}$ B _{3u}	78
		$\nu_{1,\text{LO}}$ E _g	420	ν_3 E _g	295	ν_3 E _g	327	$\nu_{3,\text{TO}}$ B _{1u}	354	$\nu_{2,\text{TO}}$ B _{3u}	259
		$\nu_{2,\text{LO}}$ E _g	446	ν_4 E _g	408	ν_4 E _g	595	$\nu_{3,\text{LO}}$ B _{1u}	354	$\nu_{2,\text{LO}}$ B _{3u}	267
		$\nu_{3,\text{LO}}$ E _g	602	ν_5 E _g	500			$\nu_{4,\text{TO}}$ B _{1u}	472	$\nu_{3,\text{TO}}$ B _{3u}	302
		$\nu_{4,\text{LO}}$ E _g	766	ν_6 E _g	610			$\nu_{4,\text{LO}}$ B _{1u}	492	$\nu_{3,\text{LO}}$ B _{3u}	89
		$\nu_{1,\text{TO}}$ A _{1g}	538	$\nu_{1,\text{LO}}$ E _u	660			$\nu_{5,\text{TO}}$ B _{1u}	570	$\nu_{4,\text{TO}}$ B _{3u}	411
		$\nu_{2,\text{TO}}$ A _{1g}	613	$\nu_{2,\text{LO}}$ E _u	1320			$\nu_{5,\text{LO}}$ B _{1u}	570	$\nu_{4,\text{LO}}$ B _{3u}	585
		$\nu_{1,\text{LO}}$ A _{1g}	602					$\nu_{6,\text{TO}}$ B _{1u}	974	$\nu_{5,\text{TO}}$ B _{3u}	766
		$\nu_{2,\text{LO}}$ A _{1g}	759					$\nu_{6,\text{LO}}$ B _{1u}	1040	$\nu_{5,\text{LO}}$ B _{3u}	965
								$\nu_{1,\text{TO}}$ B _{2u}	213	$\nu_{6,\text{TO}}$ B _{3u}	981
								$\nu_{1,\text{LO}}$ B _{2u}	226	$\nu_{6,\text{LO}}$ B _{3u}	987
								$\nu_{2,\text{TO}}$ B _{2u}	285		
								$\nu_{2,\text{LO}}$ B _{2u}	314		

		E _{HF} (%)	0.00	0.00	0.00	0.00	20.00	20.00	20.00	25.00	25.00	25.00	25.00	27.00	33.33	60.00
TMOs	Mode	ω_v	PBE	BLYP	PBESOL	M06L	B3PW	B3PBE	B3LYP	PBE0	PBESOLO	HSE06	HSESOL	M06	PBE0-13	HISS
CoO	E _u	350	346.67	355.98	320.78	378.74	376.95	389.39	357.68	389.26	407.37	385.43	406.68	N/A	433.59	397.93
CuO	B _{2u}	530	476.80	459.91	503.20	482.00	544.42	547.83	537.93	542.37	557.97	540.65	556.28	548.76	540.27	548.30
Cu ₂ O	F _{1u}	634	605.34	568.54	649.48	636.28	615.05	631.66	587.61	620.60	653.00	620.10	652.76	615.88	623.63	632.37
Cr ₂ O ₃	E _g	444	408.17	406.98	414.35	421.83	437.73	438.73	436.84	443.33	448.25	N/A	N/A	442.76	452.84	N/A
Fe ₂ O ₃	E _g	408	378.37	371.54	379.68	421.05	416.26	420.73	411.81	422.79	525.06	421.50	432.49	421.59	433.52	437.44
MnO	E _u	258	156.92	126.08	147.67	183.63	248.04	255.27	231.55	264.23	274.97	260.81	271.95	242.94	282.34	288.99
NiO	E _u	387	370.59	344.63	400.19	393.20	401.68	381.84	380.60	410.43	435.56	409.50	434.23	393.60	418.75	422.84
V ₂ O ₅	B _{2u}	506	419.48	427.06	449.30	428.83	493.29	522.34	507.28	522.71	528.40	519.98	527.03	519.96	530.57	528.79
V ₂ O ₃	A _{1g}	501	478.66	459.88	505.22	472.75	490.74	500.08	511.91	498.41	516.30	N/A	N/A	490.14	508.30	N/A
ZnO	E _{1u}	407	398.20	382.70	423.16	417.25	421.27	429.34	409.12	427.19	445.29	426.24	444.08	411.07	435.61	440.22
TiO ₂	A _{1g}	612	575.65	559.99	598.91	608.82	605.11	613.10	594.08	614.44	630.99	613.17	629.70	599.05	627.25	633.48

Figure S9: Calculated harmonic phonon vibrations at the Γ point for the selected modes of TMOs according to S1. N/A correspond to calculations that did not converge. The cyan box in V₂O₅ for PBE0-1/3 only converged with no D3-BJ, and in HISS D3-BJ is not available.

Table S2: Table showing phonon vibrations at the Γ point: TMOs number of modes with imaginary frequencies (yellow), TMOs with one negative eigenvalue without imaginary frequency (*), and N/A indicates phonon calculations that did not converge.

TMOs	PBE	BLYP	PBESOL	M06L	B3PW	B3PBE	B3LYP	PBE0	PBESOLO	PBE0-13	M06	HSE06	HISS	HSESOL
CoO	0	0	0	*	0	*	0	*	*	*	N/A	0	0	*
CuO	0	0	0	0	0	0	0	0	0	0	0	0	0	0
Cu ₂ O	0	0	0	0	0	0	*	0	0	0	*	0	0	*
Cr ₂ O ₃	0	0	0	0	0	0	0	0	0	0	0	N/A	N/A	N/A
Fe ₂ O ₃	0	0	0	0	0	0	0	0	0	0	0	0	0	0
MnO	0	0	0	0	0	0	0	0	0	0	0	0	0	0
NiO	*	0	0	*	0	0	*	0	0	0	0	*	0	0
V ₂ O ₅	0	0	0	0	0	5	5	5	5	5	5	5	*	5
V ₂ O ₃	0	0	0	0	0	0	0	0	0	0	0	N/A	N/A	N/A
ZnO	*	*	0	*	*	*	*	*	0	*	*	0	0	*
TiO ₂	3	4	1	0	3	1	4	3	0	*	4	*	0	0

5 Electronic Properties

5.1 Band Structure and Density of States



Figure S10: Band gap (E_g) values calculated with different density functionals. Experimental data (first column) references: CoO,^{48–50} CuO,^{51,52} Cu₂O,⁵³ Cr₂O₃,^{54,55} Fe₂O₃,⁵⁶ MnO,^{48,49,57} NiO,^{48,58} V₂O₅,^{59,60} ZnO,⁶¹ TiO₂.⁵⁹

Table S3: Calculated exchange energy ΔE_X in $\text{kcal}\cdot\text{mol}^{-1}$ for magnetic phase transition with different XC functionals. The spin transition is from ferromagnetic (FM) to antiferromagnetic (AFII) of rock salt structure CoO, NiO and MnO.

DF	$\Delta E_{\text{FM} \rightarrow \text{AFM}}$ (kcal/mol)		
	CoO	NiO	MnO
BLYP	-0.48	-6.33	-4.33
PBE	-5.02	-6.70	-4.30
PBESOL	-6.28	-6.80	-4.26
M06L	-3.13	-3.68	-2.22
B3PW	-1.71	-2.67	-1.93
B3PBE	-25.88	-2.80	-2.58
B3LYP	-27.55	-2.65	-1.95
PBEO	-15.03	-2.26	-1.71
PBESOLO	-31.12	-3.82	-1.97
PBEO-1/3	-19.08	-1.78	-2.18
M06	1.03	-2.87	-0.71
HSE06	-22.18	-2.38	-1.82
HSESOL	-12.78	-3.47	-2.08
HISS	-30.77	-2.01	-1.72

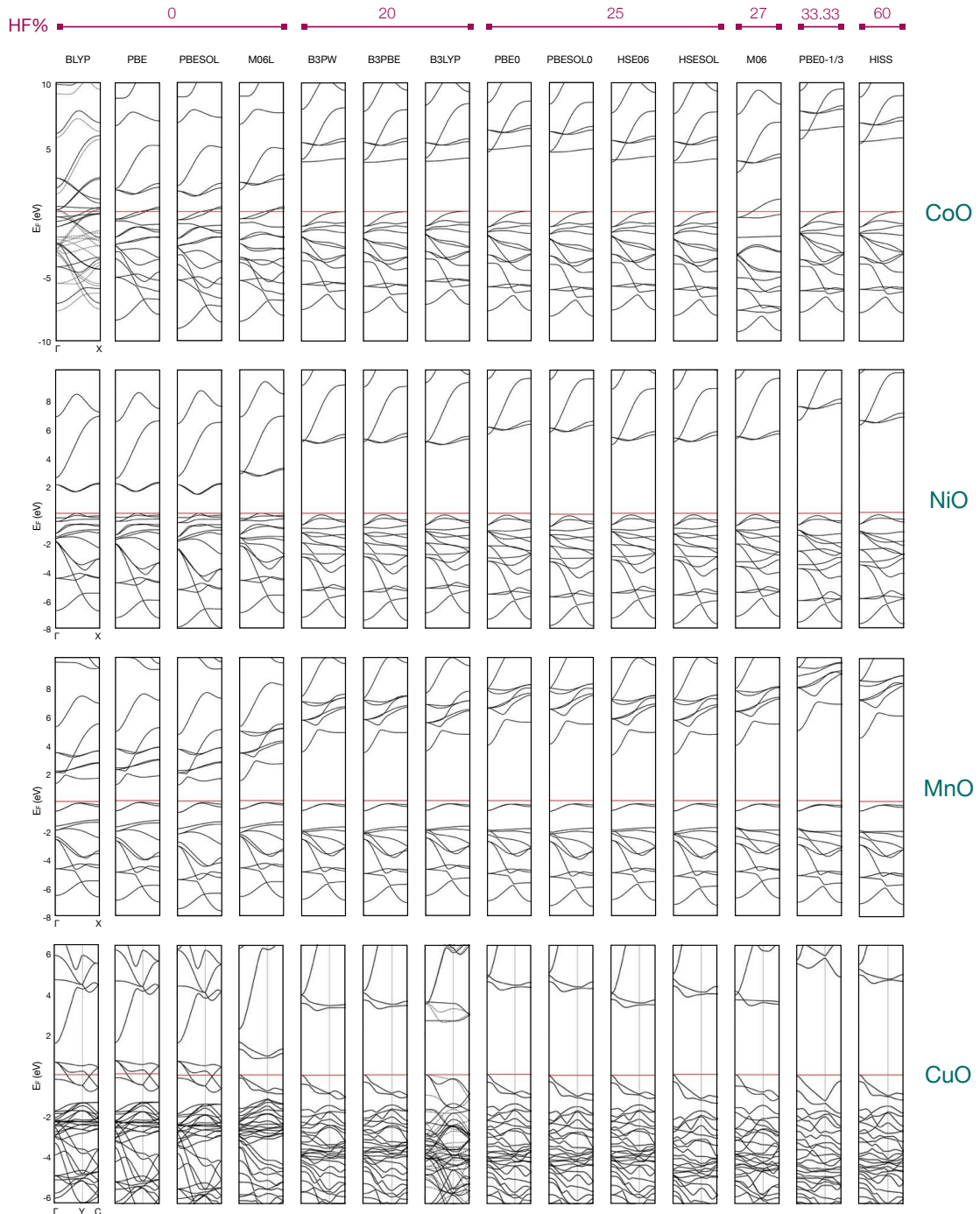


Figure S11: Band structure in the first path of the Brillouin zone for open-shell transition metal monoxides, cubic systems CoO, NiO, and MnO, and first two paths for monoclinic CuO. The lines and numbers at the top show the amount of E_{HF} exchange for each density functional.



Figure S12: Band structure in the first path of the Brillouin zone for open-shell transition metal trioxide trigonal systems V_2O_3 , Fe_2O_3 , Cr_2O_3 . The lines and numbers at the top show the amount of E_{HF} exchange for each density functional.

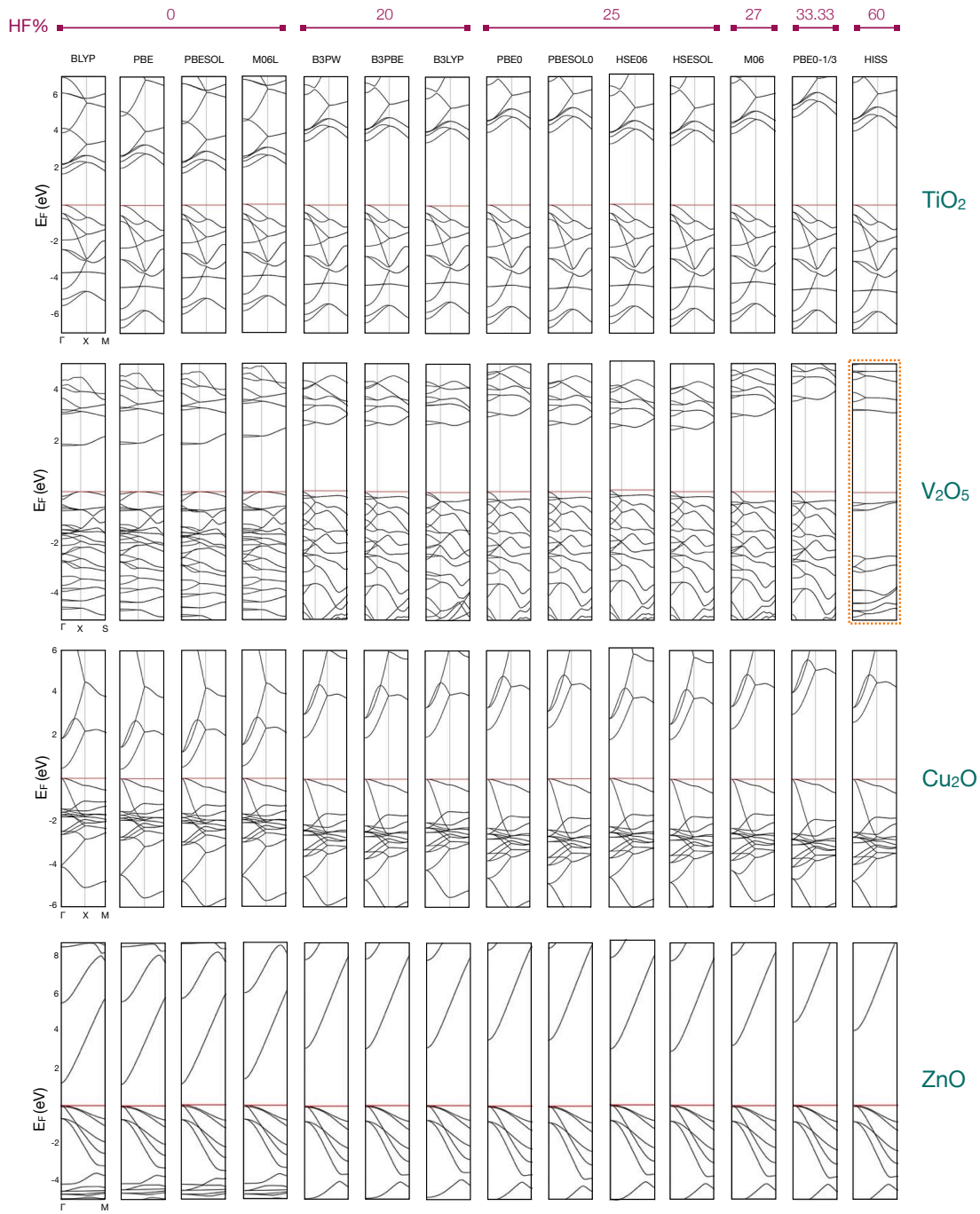


Figure S13: Band structure in the first path of the Brillouin zone for closed-shell transition metal trigonal ZnO , and the first two paths for tetragonal TiO_2 , orthorombic V_2O_5 , and cubic Cu_2O . The lines and numbers at the top show the amount of E_{HF} exchange for each density functional. The band path circled in yellow (HISS) in V_2O_5 does not include D3 corrections.

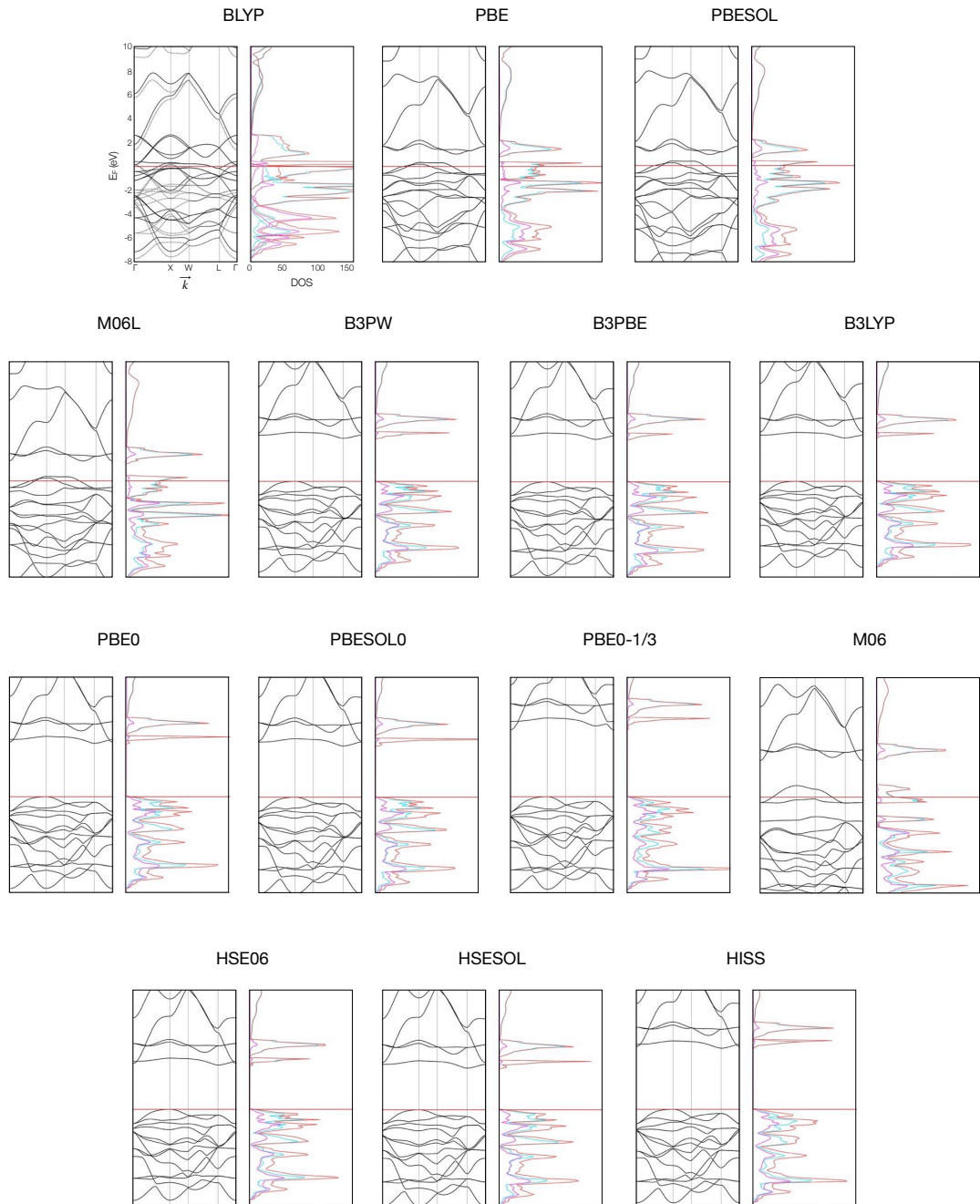


Figure S14: Band structure and density of states for CoO calculated with different density functionals. Color-code DOS projections: *red* = total, *light blue* = cobalt, *pink* = oxygen.



Figure S15: Band structure and density of states for Cr_2O_3 calculated with different density functionals. Color-code DOS projections: *red* = total, *light blue* = chromium, *pink* = oxygen.

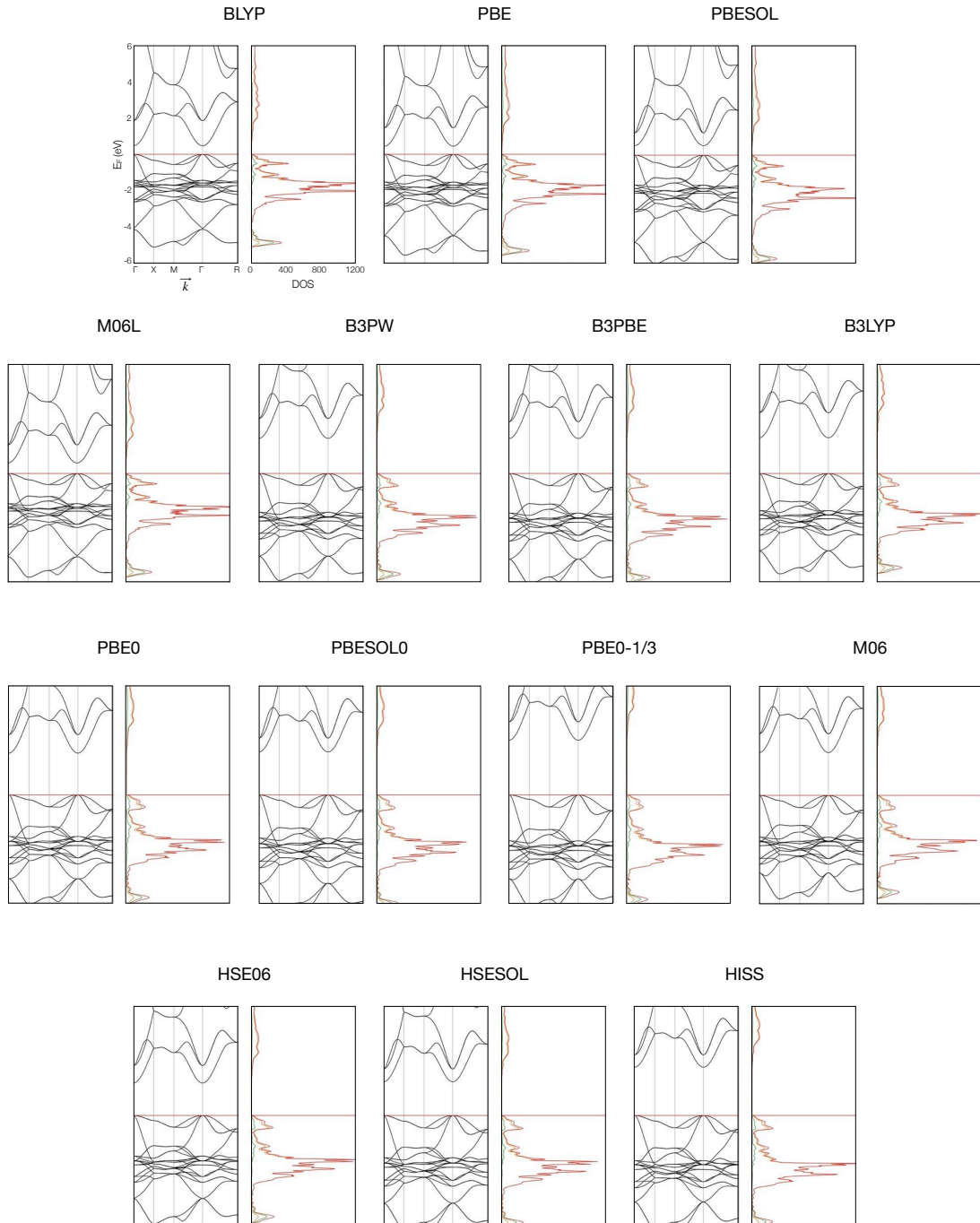


Figure S16: Band structure and density of states for Cu_2O calculated with different density functionals. Color-code DOS projections: *red* = total, *orange* = copper, *green* = oxygen.

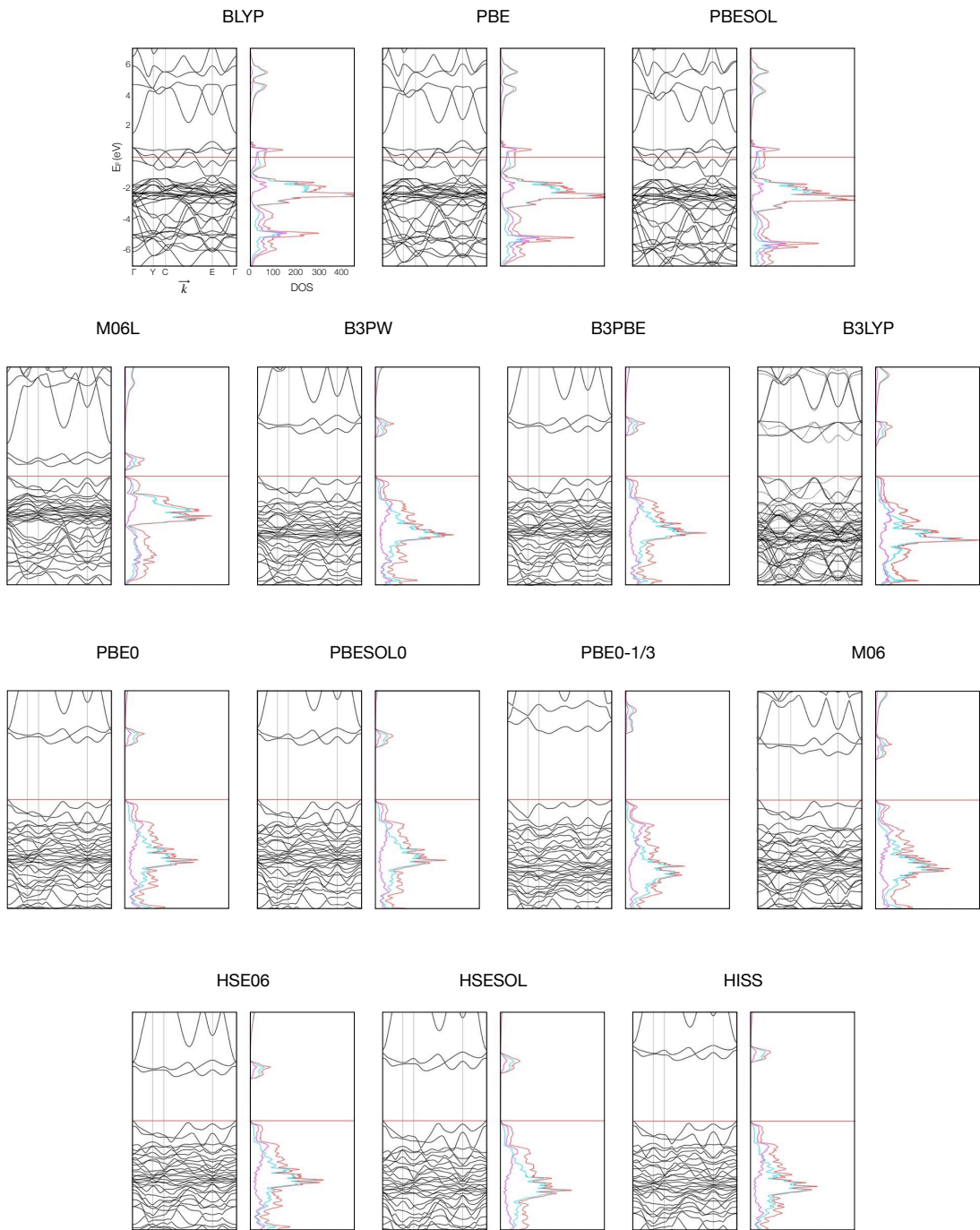


Figure S17: Band structure and density of states for CuO calculated with different density functionals. Color-code DOS projections: *red* = total, *light blue* = copper, *pink* = oxygen.



Figure S18: Band structure and density of states for Fe_2O_3 calculated with different density functionals. Color-code DOS projections: *red* = total, *light blue* = iron, *pink* = oxygen.

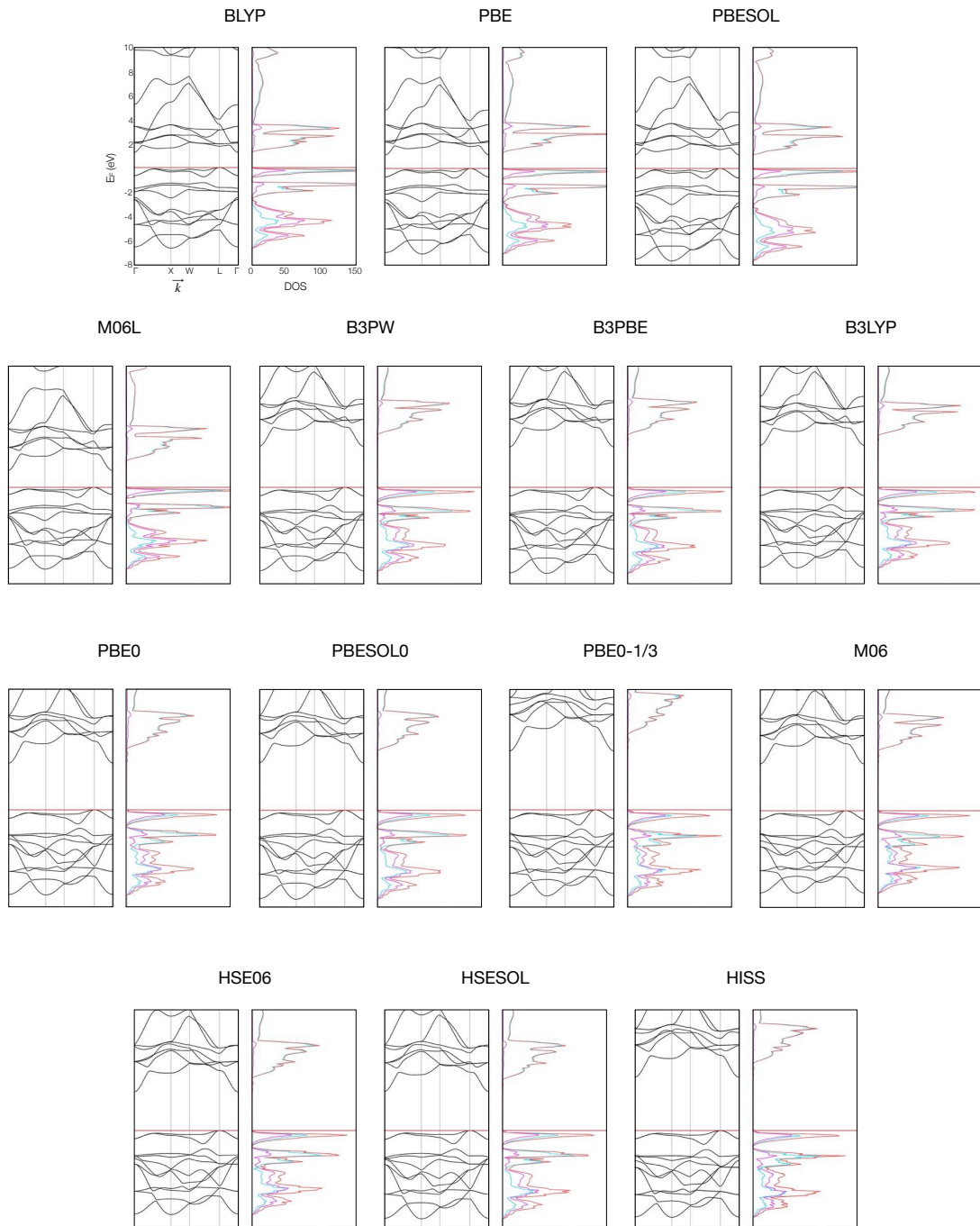


Figure S19: Band structure and density of states for MnO calculated with different density functionals. Color-code DOS projections: *red* = total, *light blue* = manganese, *pink* = oxygen.

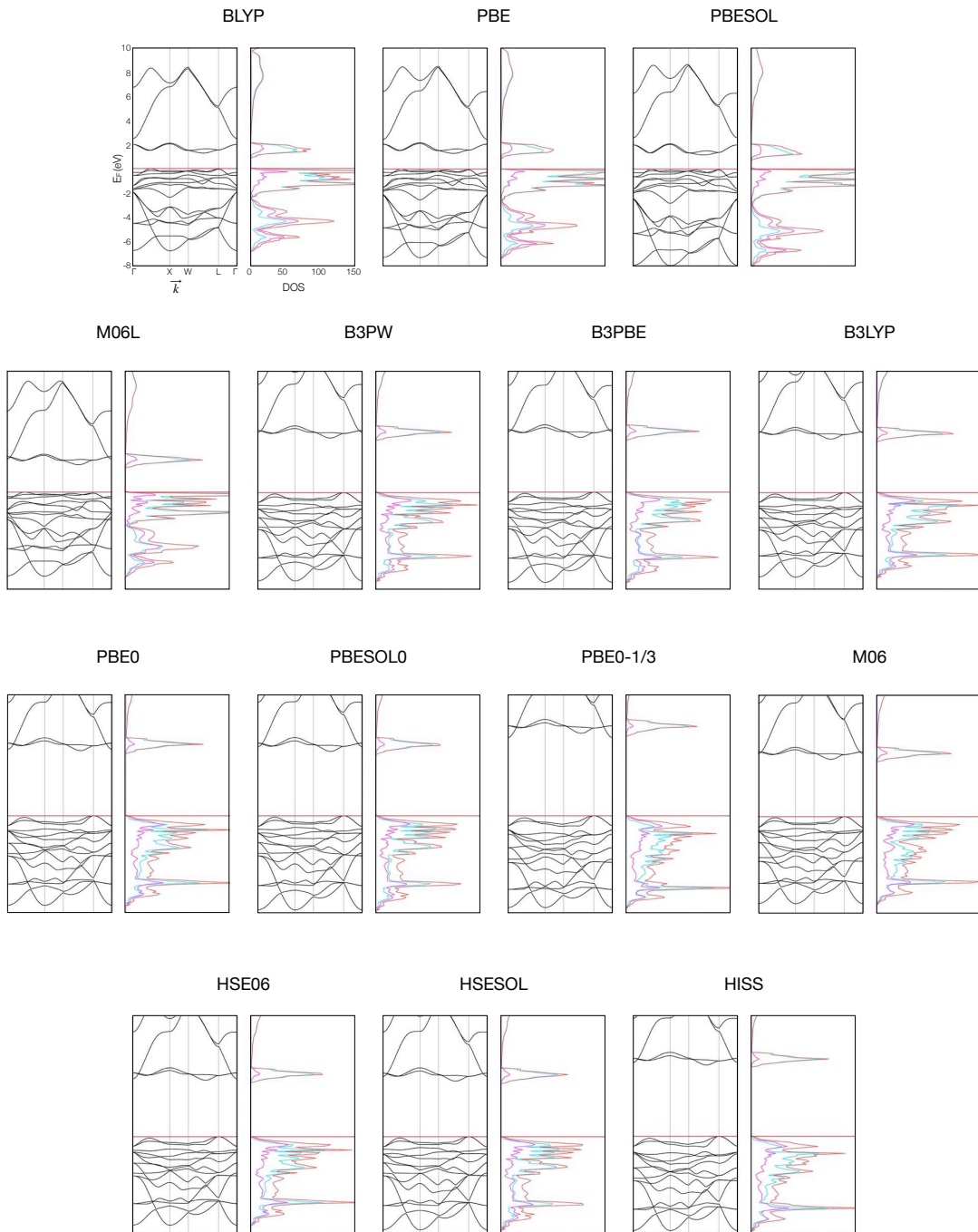


Figure S20: Band structure and density of states for NiO calculated with different density functionals. Color-code DOS projections: *red* = total, *light blue* = nickel, *pink* = oxygen.



Figure S21: Band structure and density of states for TiO₂ calculated with different density functionals. Color-code DOS projections: *light green* = total, *pale pink* = titanium, *grey* = oxygen.



Figure S22: Band structure and density of states for V_2O_3 calculated with different density functionals. Color-code DOS projections: *red* = total, *light blue* = vanadium, *pink* = oxygen.

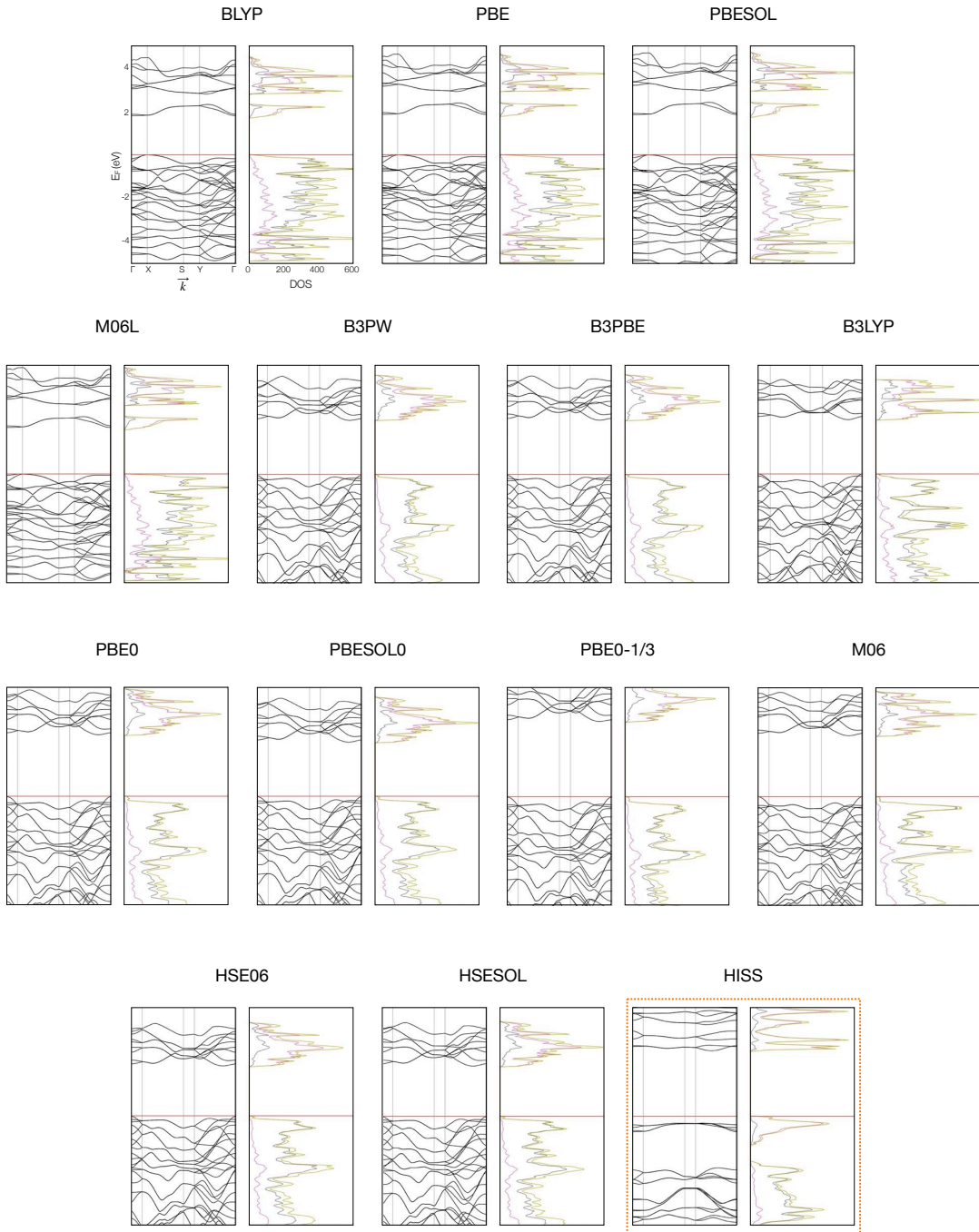


Figure S23: Band structure and density of states for V_2O_5 calculated with different density functionals. Color-code DOS projections: *light green* = total, *pale pink* = vanadium, *grey* = oxygen.

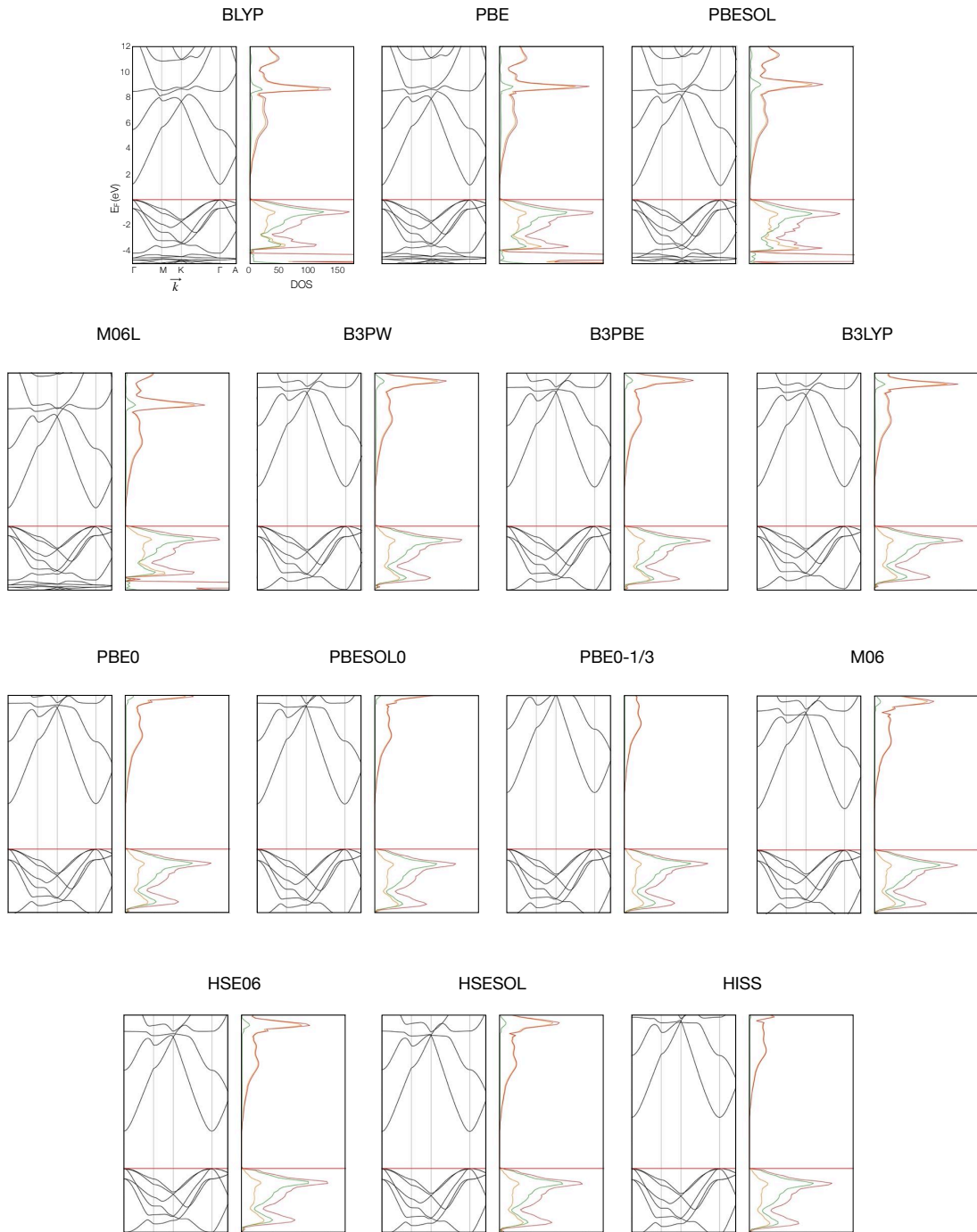


Figure S24: Band structure and density of states for ZnO calculated with different density functionals. Color-code DOS projections: *red* = total, *orange* = zinc, *green* = oxygen.

5.1.1 Magnetic Moment and Charges

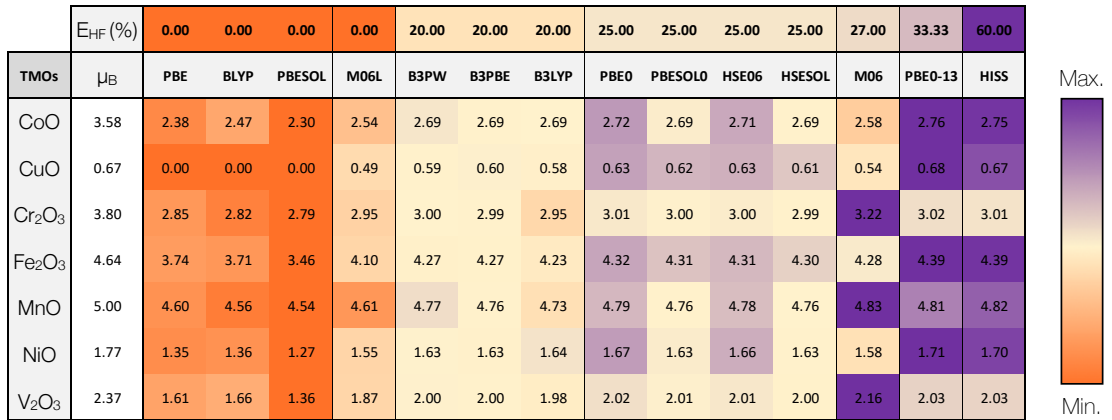


Figure S25: Magnetic moment (μ_B) values calculated with different density functionals. Experimental data (first column) references: CoO,^{62,63} CuO,⁶² Cr₂O₃,⁶⁴ Fe₂O₃,^{62,65} MnO,^{63,66} NiO,^{62,63,66} V₂O₃.⁶⁷

To understand how the different DFs affect charge distribution and the nature of the TM-O bonding, a colormap describing electron distribution around atoms is shown in Figure S28. The values in Figure S28 are the TMO charge differences (ΔQ_{TMO}), defined as the difference between TM (δq_{TM}) and O (δq_O) partial charges obtained through the Mulliken population analysis:

$$\Delta Q_{TMO} = \delta q_{TM} - \delta q_O \quad (17)$$

The Mulliken population analysis is an orbital-based approach that separates the charge population near a nucleus into atomic orbitals and overlap populations. Colormaps for the partial charges of the TM and oxygen in the TMOs are available in Figures S26 and S27.

In Figure S28, the color scale is applied to each row in the colormap separately, to illustrate how charge populations change as a function of the DF, since it is not meaningful to compare the character of the TM-O bonding between TMOs, as they are unique. The nature of the TM-O bond varies between more covalent-like and more ionic-like bonding character, reflecting differences in the electron density charge delocalization. In the colormap, blue indicate a higher partial charge difference between the metal and the oxygen, therefore a more ionic character, while yellow colors indicate more covalent-like character, corresponding to lower partial charge differences and thus bonds where the electrons tend to be more distributed between the atoms.

The bonding in TMOs is primarily ionic with some back-donation of charge from filled oxygen orbitals to the TM atoms. This back-donation introduces some covalent bonding character reducing the ionic charges, and changing in magnitude the bonding strength in the different TMOs systems.⁶⁸ The colormap in Figure S28 shows that the calculated bond ionicity depends on the choice of the XC functional. At the top of the figure, the amount E_{HF} in each DF is indicated to highlight how addition of exact exchange influences electron delocalization. For the semi-local approximations with no inclusion of E_{HF} , namely PBE, BLYP, PBESOL and M06L, delocalization errors play an important role and the bonding tends toward covalency, indicated by the dark yellow colors. On the other hand, addition of larger amounts of E_{HF} seems to shift electron delocalization towards a higher ionic character, indicated by the blue colors. The lighter shades of yellow/blue are for the intermediate cases of the global hybrids and RSH with E_{HF}

$E_{HF}(\%)$	0.00	0.00	0.00	0.00	20.00	20.00	20.00	25.00	25.00	25.00	25.00	27.00	33.33	60.00
TMOs	PBE	BLYP	PBESOL	M06L	B3PW	B3PBE	B3LYP	PBE0	PBESOLO	HSE06	HSESOL	M06	PBE0-13	HISS
CoO	1.57	1.70	1.54	1.59	1.94	1.91	2.01	1.97	1.96	1.97	1.96	1.84	2.07	2.15
CuO	1.33	1.36	1.32	1.47	1.68	1.66	1.70	1.74	1.72	1.73	1.72	1.56	1.87	1.90
Cu ₂ O	1.20	1.21	1.23	1.29	1.35	1.34	1.35	1.37	1.39	1.37	1.39	1.26	1.42	1.45
Cr ₂ O ₃	2.25	2.36	2.21	2.36	2.62	2.58	2.68	2.66	2.65	2.66	2.65	2.60	2.80	2.86
Fe ₂ O ₃	1.92	1.99	1.82	2.18	2.34	2.30	2.39	2.40	2.36	2.39	2.35	2.30	2.53	2.57
MnO	1.70	1.82	1.67	1.66	1.99	1.95	2.06	2.01	1.99	2.01	1.99	1.95	2.09	2.17
NiO	1.53	1.63	1.51	1.55	1.92	1.88	1.98	1.96	1.94	1.96	1.94	1.80	2.07	2.14
V ₂ O ₅	2.20	2.22	2.15	2.30	2.10	2.05	2.17	2.12	2.05	2.12	2.05	2.14	2.21	2.19
V ₂ O ₅ *	2.21	2.25	2.16	2.14	2.11	2.04	2.19	2.13	1.99	2.12	2.06	2.17	2.24	N/A
V ₂ O ₃	2.17	2.29	2.10	2.33	2.55	2.50	2.61	2.59	2.55	2.58	2.54	2.54	2.71	2.77
ZnO	1.72	1.73	1.68	1.87	1.92	1.90	1.92	1.96	1.92	1.95	1.92	1.78	2.03	2.08
TiO ₂	2.64	2.71	2.55	2.92	2.90	2.86	2.95	2.94	2.87	2.95	2.88	2.93	3.04	3.10

Figure S26: Absolute values of Mulliken population charges on the transition metal of the TMOs.

$E_{HF}(\%)$	0.00	0.00	0.00	0.00	20.00	20.00	20.00	25.00	25.00	25.00	25.00	27.00	33.33	60.00
TMOs	PBE	BLYP	PBESOL	M06L	B3PW	B3PBE	B3LYP	PBE0	PBESOLO	HSE06	HSESOL	M06	PBE0-13	HISS
CoO	-0.79	-0.85	-0.77	-0.79	-0.97	-0.95	-1.00	-0.98	-0.98	-0.99	-0.98	-0.92	-1.04	-1.08
CuO	-0.67	-0.68	-0.66	-0.74	-0.84	-0.83	-0.85	-0.87	-0.86	-0.87	-0.86	-0.78	-0.94	-0.95
Cu ₂ O	-0.80	-0.81	-0.82	-0.86	-0.90	-0.90	-0.90	-0.91	-0.92	-0.91	-0.93	-0.84	-0.94	-0.97
Cr ₂ O ₃	-0.90	-0.94	-0.88	-0.94	-1.05	-1.03	-1.07	-1.07	-1.06	-1.07	-1.06	-1.04	-1.12	-1.14
Fe ₂ O ₃	-0.77	-0.80	-0.73	-0.87	-0.94	-0.92	-0.95	-0.96	-0.94	-0.96	-0.94	-0.92	-1.01	-1.03
MnO	-0.85	-0.91	-0.84	-0.83	-1.00	-0.97	-1.03	-1.00	-0.99	-1.01	-1.00	-0.97	-1.05	-1.09
NiO	-0.77	-0.82	-0.75	-0.78	-0.96	-0.94	-0.99	-0.98	-0.97	-0.98	-0.97	-0.90	-1.04	-1.07
V ₂ O ₅	-0.78	-0.78	-0.76	-0.66	-0.59	-0.57	-0.60	-0.59	-0.57	-0.59	-0.57	-0.60	-0.61	-0.55
V ₂ O ₅ *	-0.78	-0.79	-0.76	-0.50	-0.60	-0.58	-0.63	-0.60	-0.56	-0.60	-0.58	-0.61	-0.63	N/A
V ₂ O ₃	-0.87	-0.92	-0.84	-0.93	-1.02	-1.00	-1.04	-1.03	-1.02	-1.03	-1.02	-1.02	-1.08	-1.11
ZnO	-0.86	-0.87	-0.84	-0.94	-0.96	-0.95	-0.96	-0.98	-0.96	-0.98	-0.96	-0.89	-1.01	-1.04
TiO ₂	-0.88	-0.90	-0.85	-0.97	-0.97	-0.95	-0.98	-0.98	-0.96	-0.98	-0.96	-0.98	-1.01	-1.03

Figure S27: Absolute values of Mulliken population charges on the oxygen of the TMOs.

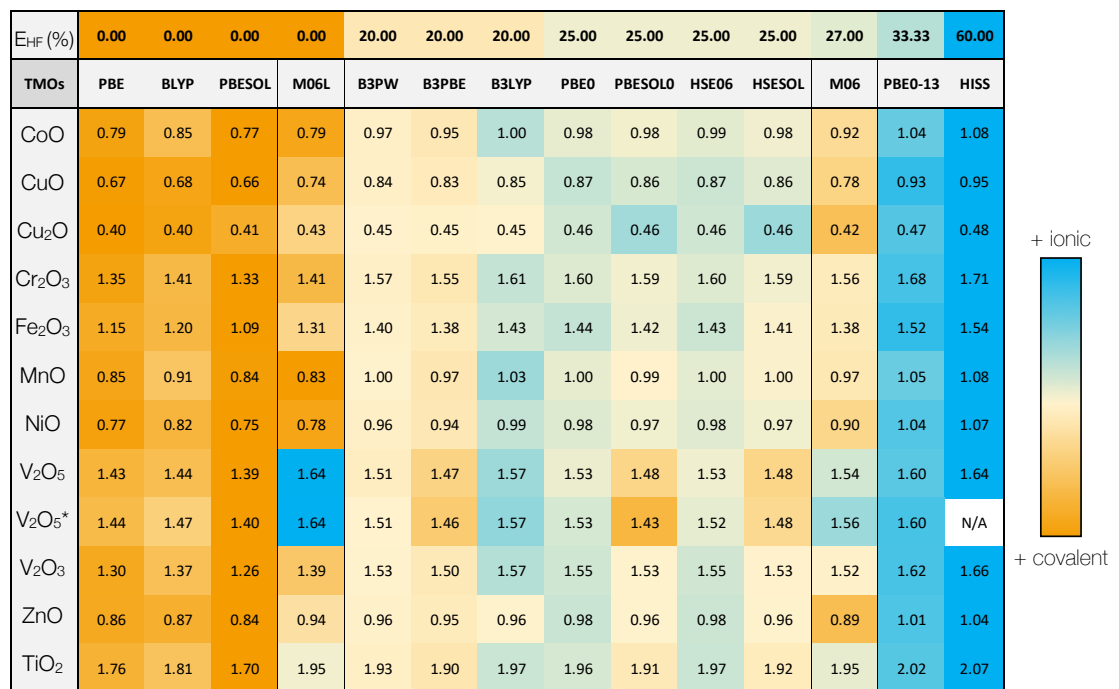


Figure S28: Colormap showing the differences between the transition metal and oxygen partial charges; the color scale indicates the tendency towards more ionic or covalent nature of TM-O bonding. The layered structure V₂O₅* includes D3-BJ corrections.

ranging between 20 and 25 %. There is no significant difference in colors and values between PBE0/PBESOL0 and HSE06/HSESOL, suggesting that the short-range screened functionals produce similar charge distributions as the global hybrids. For M06, a generally stronger yellow color indicates that the hybrid mGGA has a tendency to describe the nature of TM-O bond as more covalent, regardless of the fact that it contains 27 % of E_{HF} .

The higher partial charge differences for B3LYP (indicated by the blue colors), in comparison to B3PW and B3PBE (light yellow colors), show that the correlation part of this XC functional shifts the bonding slightly towards being more ionic. The partial charge differences for the layered structure V_2O_5 , and $V_2O_5^*$ with D3-BJ corrections, show an interesting effect. The semi-local approximations, particularly PBE and BLYP, mostly produce a more ionic character, as does M06L when dispersion corrections are not included. All global hybrids, except for B3LYP, tend towards more covalency (bright yellow). The bonding nature shifts towards more ionic character again for XC functionals with the highest values of E_{HF} , PBE0-1/3 and HISS. This is in stark contrast to the results for other TMOs; specifically, the change in bond character between the semi-local approximations and the global hybrids is reversed for V_2O_5 and $V_2O_5^*$ compared with the other TMOs. This anomalous behavior of the layered TMO was also noted in the discussion of E_g and, as previously mentioned, is an interesting topic for further investigation.

Charge distribution schemes can indicate the locations where electrons tend to accumulate or be depleted. This can be used, for example, to understand electron density in a material's surface and hence to map where molecular species are most likely to interact at the surface of a material, which is useful for many applications, including catalysis.

5.1.2 Spin Contamination

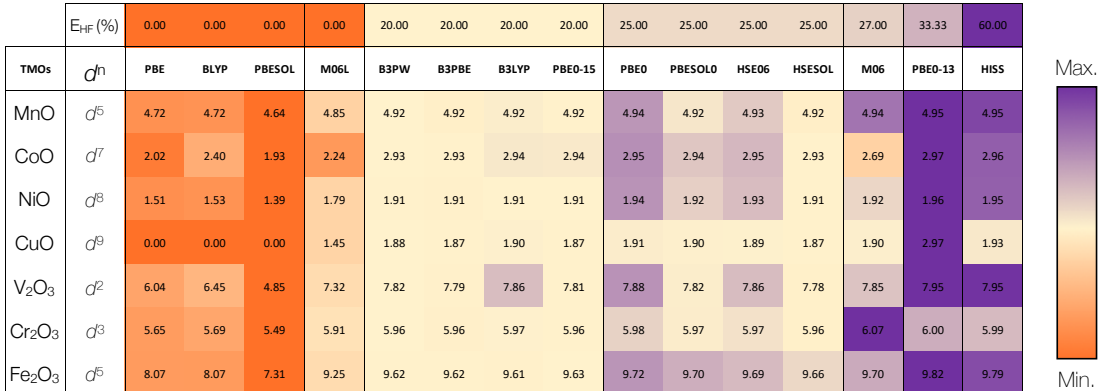


Figure S29: Colormap showing the predicted spin operator $\langle \hat{S}^2 \rangle_{UKS}$; the color scale indicates lowest (orange), midpoint (yellow), highest (purple) calculated values for each open-shell TMO.

5.2 Optical Properties

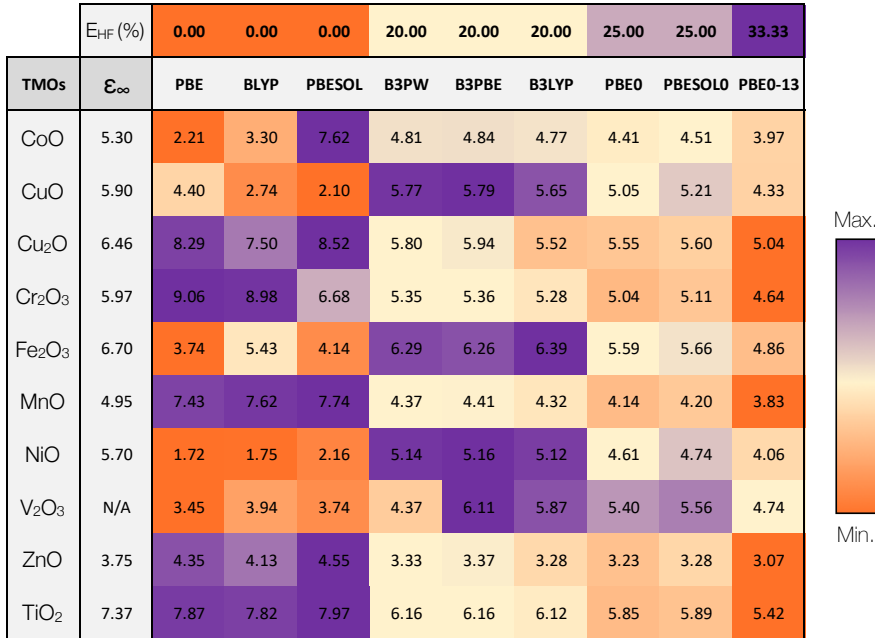


Figure S30: High frequency dielectric constants (ϵ_{∞}) calculated through Coupled-Perturbed Kohn-Sham (CPKS) scheme, compared to experimental values. Experimental data (first column) references: CoO,^{39,69} CuO ($\parallel b$ axis),^{30,70} Cu₂O,²⁸ Cr₂O₃ ($\parallel c$ axis),⁷¹ Fe₂O₃,⁴⁴ MnO,^{38,69} NiO,^{40,69} ZnO ($\parallel c$ axis),^{72–74} and TiO₂ (average along a , b , and c).^{75,76}

6 Average Performances

	$E_{HF} (\%)$	0.00	0.00	0.00	20.00	20.00	20.00	25.00	25.00	33.33
TMOs	n	PBE	BLYP	PBESOL	B3PW	B3PBE	B3LYP	PBE0	PBESOLO	PBE0-13
CoO	N/A	2.33	5.57	2.76	2.19	2.20	2.18	2.10	2.12	1.99
CuO	2.63	3.03	5.01	3.51	2.40	2.40	2.37	2.25	2.28	2.08
Cu ₂ O	2.84	2.88	2.74	2.92	2.41	2.44	2.35	2.35	2.37	2.24
Cr ₂ O ₃	N/A	3.01	3.00	3.15	2.31	2.32	2.30	2.24	2.26	2.15
Fe ₂ O ₃	2.91	6.07	7.31	6.39	2.50	2.50	2.52	2.36	2.38	2.20
MnO	2.16	2.72	2.76	2.78	2.09	2.10	2.08	2.04	2.05	1.96
NiO	2.37	4.15	4.18	4.65	2.27	2.27	2.26	2.15	2.18	2.01
V ₂ O ₃	2.80	3.45	2.42	4.93	2.78	2.47	2.42	2.32	2.36	2.18
ZnO	2.01	2.08	2.03	2.13	1.82	1.83	1.81	1.80	1.81	1.75
TiO ₂	2.61	2.80	2.79	2.82	2.48	2.48	2.47	2.42	2.42	2.32

Figure S31: Refractive indices (n) calculated through the Coupled-Perturbed Kohn-Sham (CPKS) scheme, compared to experimental values. Experimental data (first column) references: CuO,^{77,78} Cu₂O,⁷⁷ Fe₂O₃,^{61,79} MnO,^{77,79} NiO,⁷⁷ V₂O₃,⁸⁰ ZnO,^{61,77,79} and TiO₂.^{61,77,79,81}

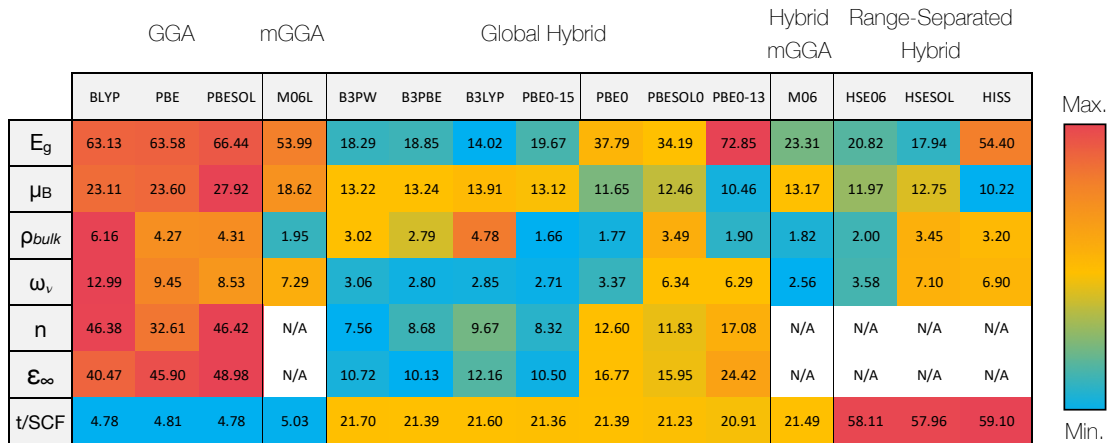


Figure S32: Colormap showing the average of absolute approximation error (δ_{avg}) for band gap (E_g), magnetic moment (μ_B), bulk density (ρ_{bulk}), vibrational frequency (ω_ν), refractive index (n), dielectric constant (ϵ_∞), and computational cost (t/SCF).

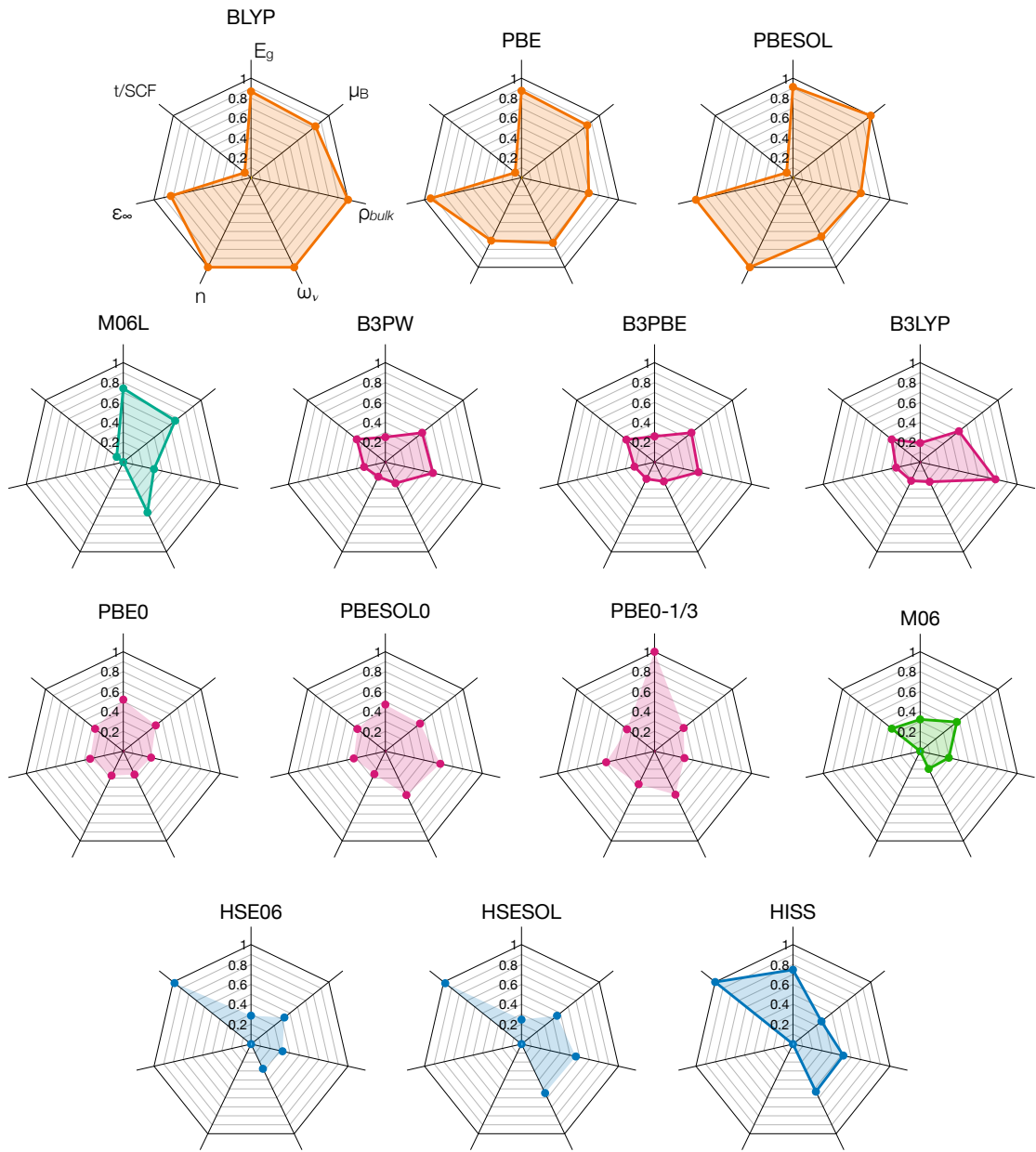


Figure S33: Spider plots of normalized average of absolute approximation error (δ_{avg}) for band gap (E_g), magnetic moment (μ_B), bulk density (ρ_{bulk}), vibrational frequency (ω_ν), refractive index (n), dielectric constant (ε_∞), and computational cost (t/SCF).

7 Input Details

7.1 Geometry Input Files

TiO₂

```
CRYSTAL
0 0 0
136
4.59 2.96
2
22 .0 .0 .0
8 .305 .305 .0
OPTGEOM
FULLOPTG
END
(...)
99 0
END
DFT
(...)
END
SHRINK
8 8
TOLINTEG
8 8 8 16
TOLDEE
8
MAXCYCLE
200
FMIXING
80
EXCHSIZE
30000000
BIPOSIZE
30000000
PPAN
SCFDIR
END
```

V₂O₅

```
CRYSTAL
0 0 0
59
11.544 3.571 4.383 90.0
4
23 0.60123 0.25 0.1086
8 0.43090 0.25 -0.0028
```

```

8 0.10450 0.25 0.4697
8 0.75000 0.25 0.4697
OPTGEOM
FULLOPTG
END
END
(...)
99 0
END
DFT
(...)
END
SHRINK
8 8
TOLINTEG
8 8 8 16
TOLDEE
8
MAXCYCLE
200
FMIXING
90
EXCHSIZE
30000000
BIPOSIZE
30000000
PPAN
SCFDIR
END

```

V₂O₃

```

CRYSTAL
1 0 0
P 1 2/c 1
5.54800 5.00200 7.25500 96.75000
6
23 0.29930 -0.00120 0.34390
23 0.79930 0.49880 0.84390
8 0.15100 0.65300 -0.09400
8 0.65100 0.15300 0.40600
8 0.00000 0.80400 0.25000
8 0.50000 0.69600 0.25000
OPTGEOM
FULLOPTG
END
END
(...)
```

```
99 0
END
DFT
(...)
SPIN
END
SHRINK
8 8
TOLINTEG
8 8 8 8 16
TOLDEE
8
ATOMSPIN
8
1 -1 2 -1 3 -1 4 -1 5 1 6 1 7 1 8 1
MAXCYCLE
200
FMIXING
80
EXCHSIZE
30000000
BIPOSIZE
30000000
PPAN
SCFDIR
END
```

Cr₂O₃

```
CRYSTAL
0 0 0
167
4.9570 13.5923
2
24 0.0 0.0 0.34751
8 0.3057 0.0 0.25
SYMMREMO
OPTGEOM
FULLOPTG
END
END
(...)
99 0
END
DFT
(...)
SPIN
END
```

```
SHRINK
8 8
TOLINTEG
8 8 8 8 16
TOLDEE
8
ATOMSPIN
4
1 1 2 -1 3 1 4 -1
MAXCYCLE
200
FMIXING
90
EXCHSIZE
30000000
BIPOSIZE
30000000
PPAN
SCFDIR
END
```

MnO

```
CRYSTAL
0 0 0
225
4.445
2
25 0.0 0.0 0.0
8 0.5 0.5 0.5
SUPERCEL
0. 1. 1.
1. 0. 1.
1. 1. 0.
OPTGEOM
FULLOPTG
END
END
(...)
99 0
END
DFT
(...)
SPIN
END
SHRINK
8 8
TOLINTEG
```

```
8 8 8 8 16
TOLDEE
8
ATOMSPIN
2
1 1 2 -1
MAXCYCLE
200
FMIXING
80
EXCHSIZE
30000000
BIPOSIZE
30000000
PPAN
SCFDIR
END
```

Fe₂O₃

```
CRYSTAL
0 0 0
161
5.07872491 13.64420305
3
26 3.33333333333E-01 -3.33333333333E-01 2.479007691805E-02
26 -1.695676559034E-19 -1.073311903397E-19 1.418783418267E-01
8 3.333342514328E-01 3.625696590101E-01 -8.333391735936E-02
OPTGEOM
FULLOPTG
END
END
(...)
99 0
END
DFT
(...)
SPIN
END
SHRINK
8 8
TOLINTEG
8 8 8 8 16
TOLDEE
8
ATOMSPIN
4
1 1 2 1 3 -1 4 -1
```

```
MAXCYCLE  
200  
FMIXING  
80  
EXCHSIZE  
30000000  
BIPOSIZE  
30000000  
PPAN  
SCFDIR  
END
```

CoO

```
CRYSTAL  
0 0 0  
225  
4.260  
2  
27 0.0 0.0 0.0  
8 0.5 0.5 0.5  
SUPERCEL  
0. 1. 1.  
1. 0. 1.  
1. 1. 0.  
OPTGEOM  
FULLOPTG  
END  
END  
(...)  
99 0  
END  
DFT  
(...)  
SPIN  
END  
SHRINK  
8 8  
TOLINTEG  
8 8 8 16  
TOLDEE  
8  
ATOMSPIN  
2  
1 1 2 -1  
MAXCYCLE  
200  
FMIXING
```

```
80
EXCHSIZE
30000000
BIPOSIZE
30000000
PPAN
SCFDIR
END
```

NiO

```
CRYSTAL
0 0 0
225
4.178
2
28 0.0 0.0 0.0
8 0.5 0.5 0.5
SUPERCEL
0. 1. 1.
1. 0. 1.
1. 1. 0.
OPTGEOM
FULLOPTG
END
END
(...)
99 0
END
DFT
(...)
SPIN
END
SHRINK
8 8
TOLINTEG
8 8 8 8 16
TOLDEE
8
ATOMSPIN
2
1 1 2 -1
MAXCYCLE
200
FMIXING
80
EXCHSIZE
30000000
```

```
BIPOSIZE
30000000
PPAN
SCFDIR
END
```

Cu₂O

```
CRYSTAL
0 0 0
224
4.31752282
2
29 0.00 0.00 0.00
8 0.25 0.25 0.25
OPTGEOM
FULLOPTG
END
END
(...)
99 0
END
DFT
(...)
END
SHRINK
8 8
TOLINTEG
8 8 8 8 16
TOLDEE
8
MAXCYCLE
200
FMIXING
90
EXCHSIZE
30000000
BIPOSIZE
30000000
PPAN
SCFDIR
END
```

CuO

```
CRYSTAL
0 0 0
9
```

```

4.6927 3.4283 5.1370 90 99.546
2
29 0.25 0.2467 0.0
8 0.0104 0.4177 0.2602
SUPERCEL
1 0 1
0 1 0
-1 0 1
OPTGEOM
FULLOPTG
END
END
(...)
99 0
END
DFT
(...)
SPIN
END
SHRINK
8 8
TOLINTEG
8 8 8 16
TOLDEE
8
ATOMSPIN
4
1 1 2 -1 3 1 4 -1
MAXCYCLE
200
FMIXING
80
EXCHSIZE
30000000
BIPOSIZE
30000000
PPAN
SCFDIR
END

```

ZnO

```

CRYSTAL
0 0 0
186
3.25419751 5.18818216
2
30 3.33333333333E-01 -3.33333333333E-01 -1.177223560513E-04

```

```
8 3.3333333333E-01 -3.3333333333E-01 3.826177223561E-01
OPTGEOM
FULLOPTG
END
END
(...)
99 0
END
DFT
(...)
END
SHRINK
8 8
TOLINTEG
8 8 8 16
TOLDEE
8
MAXCYCLE
200
FMIXING
80
EXCHSIZE
30000000
BIPOSIZE
30000000
PPAN
SCFDIR
END
```

7.2 Basis Sets

The def2-TZVP basis sets⁸² optimized for periodic systems were obtained by Karttunen, Linnera, and *et al.* from different publications: oxygen and zinc,⁸³ nickel,¹⁵ copper,⁸⁴ titanium,⁸⁵ manganese and cobalt,⁶⁹ iron and vanadium.⁶² For chromium, we adapted the def2-TZVP from the TURBOMOLE to CRYSTAL format, as reported in the basis set exchange (BSE) database (www.basissetexchange.org).⁸⁶ Comparison of def2-TZVP to pob-TZVP,⁸⁷ which was developed to solids, in terms of optimized geometry parameters, band gap, and computational cost, for all TMOs showed equivalent performance and accuracy.

Oxygen

8 7	
0 0 6 2.0 1.0	
27032.382631	0.21726302465E-03
4052.3871392	0.16838662199E-02
922.32722710	0.87395616265E-02
261.24070989	0.35239968808E-01
85.354641351	0.11153519115
31.035035245	0.25588953961
0 0 2 2.0 1.0	
12.271113873	0.39768730901
4.9159842006	0.24627849430
0 0 1 0.0 1.0	
0.90086482370	1.0
0 1 1 0.0 1.0	
0.25	1.0
0 2 4 4.0 1.0	
75.300554155	0.60685103418E-02
17.743733858	0.41912575824E-01
5.5355828651	0.16153841088
2.0685535103	0.35706951311
0 2 1 0.0 1.0	
0.78238772422	1.0
0 3 1 0.0 1.0	
1.20	1.0

Titanium

22 12	
0 0 8 2. 1.	
211575.69025	.23318151011E-03
31714.945058	.18079690851E-02
7217.5476543	.93984311352E-02
2042.9394247	.38156853618E-01
665.12896208	.12374757197
238.74942264	.29208551143
92.508691001	.41226800855
36.403919209	.21090534061

0 0 4 2. 1.	
232.72624607	-.24920140738E-01
71.791209711	-.11746490087
11.158534615	.56503342318
4.6548135416	.56211101812
0 0 2 2. 1.	
6.8034629174	-.23011425503
1.1201076403	.72103186735
0 0 1 2. 1.	
.48080118839	1.0
0 0 1 0. 1.	
.15	1.0
0 2 6 6. 1.	
1063.1474732	.24690839320E-02
251.56507061	.19773345523E-01
80.408554854	.90987976672E-01
29.768193269	.25559900413
11.736830556	.40489386764
4.7142375230	.23693402558
0 2 3 6. 1.	
17.796803704	-.27878639615E-01
2.4272698680	.55672914668
.96823445537	1.0055447350
0 2 1 0. 1.	
.37056694165	1.0
0 3 4 2. 1.	
37.713384723	.11513835092E-01
10.692931184	.67246343996E-01
3.6728446990	.21484207775
1.3588590303	.38890892779
0 3 1 0. 1.	
.49213295253	.43040835243
0 3 1 0. 1.	
.16330520653	.23253305465
0 4 1 0. 1.	
.562 1.	

Vanadium

23 12	
0 0 8 2.0 1.0	
232340.65058	.23072410092E-03
34828.841170	.17888178962E-02
7926.5448691	.92992490131E-02
2243.7733046	.37761463347E-01
730.59322944	.12255909662
262.32219631	.28963508811
101.70403805	.41004702955

40.064784617	.21113610858
0 0 4 2.0 1.0	
255.24014968	-.24458116338E-01
78.804646961	-.11527205366
12.340598946	.55174749453
5.1742019219	.54504528489
0 0 2 2.0 1.0	
7.6513894469	-.22967638286
1.2639759898	.71683769077
0 0 1 2.0 1.0	
0.53861761721	1.0
0 0 1 0.0 1.0	
0.27	1.0
0 1 1 0.0 1.0	
0.13	1.0 1.0
0 2 6 6.0 1.0	
1184.2369151	.24449826729E-02
280.23075192	.19643454466E-01
89.643627137	.90796949190E-01
33.242411253	.25650768222
13.144514452	.40815393750
5.2948534140	.23860378268
0 2 3 6.0 1.0	
20.175586851	-.28241489023E-01
2.7605865197	.55574635619
1.1008900902	.99319919270
0 2 1 0.0 1.0	
0.42013310739	1.0
0 3 4 3.0 1.0	
43.861134864	.11487174238E-01
12.516021891	.68247153977E-01
4.3313854957	.21837784195
1.6138855773	.39245212296
0 3 1 0.0 1.0	
0.65	1.0
0 3 1 0.0 1.0	
0.25	1.0

Chromium

24 12	
0 0 8 2.0 1.0	
254477.8070400	0.23386945693E-03
38131.7970540	0.18142601800E-02
8675.2930607	0.94363925721E-02
2455.0099848	0.38343639367E-01
799.16217787	0.12459194837
286.90021489	0.29489696029

111.25413232	0.41846149607
43.864152636	0.21633763420
0 0 4 2.0 1.0	
279.32669173	-0.23450908111E-01
86.274732376	-0.11080370027
13.555756113	0.53028965842
5.6978112751	0.51603516947
0 0 2 2.0 1.0	
8.5636582615	-0.38109545675
1.3988296768	1.1991591436
0 0 1 2.0 1.0	
0.57288171116	1.0
0 0 1 0.0 1.0	
0.29	1.0
0 1 1 0.0 1.0	
0.13	1.0
0 2 6 6.0 1.0	1.0
1306.4398864	0.24277326185E-02
309.25311441	0.19544041017E-01
98.996273963	0.90651794553E-01
36.756916451	0.25699279154
14.566657077	0.40935504891
5.8739937432	0.23729388849
0 2 3 6.0 1.0	
22.890999695	-0.28166026613E-01
3.0855001822	0.56034120148
1.2132329118	0.98119019650
0 2 1 0.0 1.0	
0.44931680699	1.0
0 3 4 4.0 1.0	
43.720074476	0.13622964026E-01
12.391242652	0.78935180133E-01
4.2639442006	0.23833840000
1.5525221790	0.39526851122
0 3 1 0.0 1.0	
0.53761929485	1.0
0 3 1 0.0 1.0	
0.16493173074	1.0

Manganese

25 12	
0 0 8 2.0 1.0	
277185.00153	.22838385133E-03
41550.769890	.17707650375E-02
9455.9700152	.92077209994E-02
2676.5206482	.37415971825E-01
871.46687530	.12164861426

312.98306420	.28824392499
121.44454051	.41041600847
47.922598829	.21372375145
0 0 4 2.0 1.0	
303.66723163	-.24589926140E-01
93.881403187	-.11602608038
14.879421214	.55112059677
6.2865200745	.53707560756
0 0 2 2.0 1.0	
9.4858591337	-.22889262695
1.5698706158	.71196169587
0 0 1 2.0 1.0	
0.65903213608	1.0
0 0 1 0.0 1.0	
0.30	1.0
0 1 1 0.0 1.0	
0.13	1.0
0 2 6 6.0 1.0	1.0
1444.7978182	.23994136455E-02
342.06551197	.19369286864E-01
109.58400891	.90236108988E-01
40.747988173	.25745467851
16.188626566	.41272351958
6.5484505964	.24087700007
0 2 3 6.0 1.0	
25.357086437	-.28707174058E-01
3.4830168782	.55208100712
1.3858800906	.97226901379
0 2 1 0.0 1.0	
0.52555094893	1.0
0 3 4 5.0 1.0	
56.563189119	.11543245294532E-01
16.278734711	.70299845987196E-01
5.6964273914	.22450770821295
2.1411147942	.39703065434226
0 3 1 0.0 1.0	
0.78291801938	1.0
0 3 1 0.0 1.0	
0.25952311214	1.0

Iron

26 12	
0 0 8 2.0 1.0	
300784.84637	.22806273096E-03
45088.970557	.17681788761E-02
10262.516317	.91927083490E-02
2905.2897293	.37355495807E-01

946.11487137	.12151108426
339.87832894	.28818881468
131.94425588	.41126612677
52.111494077	.21518583573
0 0 4 2.0 1.0	
329.48839267	-.24745216477E-01
101.92332739	-.11683089050
16.240462745	.55293621136
6.8840675801	.53601640182
0 0 2 2.0 1.0	
10.470693782	-.22912708577
1.7360039648	.71159319984
0 0 1 1.0 1.0	
0.72577288979	1.0
0 0 1 0.0 1.0	
0.32	1.0
0 1 1 0.0 1.0	
0.14	1.0
0 2 6 6.0 1.0	
1585.3959970	.23793960179E-02
375.38006499	.19253154755E-01
120.31816501	.90021836536E-01
44.788749031	.25798172356
17.829278584	.41492649744
7.2247153786	.24207474784
0 2 3 6.0 1.0	
28.143219756	-.29041755152E-01
3.8743241412	.55312260343
1.5410752281	.96771136842
0 2 1 0.0 1.0	
0.58285615250	1.0
0 3 4 7.0 1.0	
61.996675034	.11971972255E-01
17.873732552	.73210135410E-01
6.2744782934	.23103094314
2.3552337175	.39910706494
0 3 1 0.0 1.0	
0.85432239901	.40203412228
0 3 1 0.0 1.0	
0.27869254413	.21415606743

Cobalt

27 12	
0 0 8 2.0 1.0	
325817.01553	.22568462484E-03
48839.636453	.17499397533E-02
11114.937307	.91003134097E-02

3146.1603642	.36996256837E-01
1024.4378465	.12044269621
368.02508816	.28598731649
142.91229205	.40908312004
56.482649209	.21500145739
0 0 4 2.0 1.0	
356.40298318	-.24767059678E-01
110.31165215	-.11702139134
17.659634834	.55215522200
7.5059030479	.53246877060
0 0 2 2.0 1.0	
11.501807176	-.22942470077
1.9081994606	.71180933514
0 0 1 1.0 1.0	
0.79396696891	1.0
0 0 1 0.0 1.0	
0.33	1.0
0 1 1 0.0 1.0	
0.14	1.0
0 2 6 6.0 1.0	
1731.1369144	.23905767685E-02
409.91750438	.19382999967E-01
131.45648578	.90905448509E-01
48.987439714	.26146681577
19.537078992	.42157264570
7.9287281634	.24571813557
0 2 3 6.0 1.0	
31.076017584	-.29438069973E-01
4.2835180697	.55615568168
1.7022921563	.96772195064
0 2 1 0.0 1.0	
0.64202908602	1.0
0 3 4 8.0 1.0	
68.140745239	.11983845360E-01
19.685241019	.73688540475E-01
6.9322128825	.23085496779
2.6025125694	.39281059225
0 3 1 0.0 1.0	
0.94016837302	.40203412228
0 3 1 0.0 1.0	
0.30381457794	.21415606743

Nickel

28 12	
0 0 8 2.0 1.0	
351535.72935	.22529386884E-03
52695.809283	.17468616223E-02

11992.468293	.90849992136E-02
3394.5776689	.36940748447E-01
1105.3594585	.12032819950
397.14677769	.28596715057
154.27542974	.40983020196
61.018723780	.21620642851
0 0 4 2.0 1.0	
384.45559739	-.24651279268E-01
119.04879199	-.11658505277
19.137012223	.54864126676
8.1526718562	.52640051122
0 0 2 2.0 1.0	
12.579408642	-.22797884293
2.0870866081	.70703738215
0 0 1 1.0 1.0	
0.86432568555	1.0
0 0 1 0.0 1.0	
0.35	1.0
0 1 1 0.0 1.0	
0.14	1.0 1.0
0 2 6 6.0 1.0	
1883.0907486	.23748258443E-02
445.95155320	.19289457172E-01
143.08430815	.90718211507E-01
53.372920722	.26181414117
21.321919357	.42309149832
8.6643561994	.24641686015
0 2 3 6.0 1.0	
34.144255211	-.29677129163E-01
4.7122455921	.55616824096
1.8709231845	.96357766460
0 2 1 0.0 1.0	
0.70370016267	1.0
0 3 4 9.0 1.0	
74.591603465	.12077454672E-01
21.590632752	.74637262154E-01
7.6246142580	.23236775502
2.8632206762	.39042651680
0 3 1 0.0 1.0	
1.0311063388	.39509498921
0 3 1 0.0 1.0	
0.33060760691	.21138769167

Copper

29 12	
0 0 8 2.0 1.0	
377518.79923	0.22811766128E-03

56589.984311	0.17688035931E-02
12878.711706	0.91993460227E-02
3645.3752143	0.37411016434E-01
1187.0072945	0.12189873737
426.46421902	0.28983900714
165.70660164	0.41531872174
65.598942707	0.21905799287
0 0 4 2.0 1.0	
414.41265811	-0.24682525053E-01
128.32056039	-0.11716827406
20.622089750	0.55301315941
8.7821226045	0.52242718609
0 0 2 2.0 1.0	
13.741372006	-0.22736061821
2.2431246833	0.71761210873
0 0 1 1.0 1.0	
0.89370549079	1.0
0 0 1 0.0 1.0	
0.35	1.0
0 1 1 0.0 1.0	
0.14	1.0
0 2 6 6.0 1.0	
2034.7596692	0.23524822298E-02
481.90468106	0.19134070751E-01
154.67482963	0.90171105278E-01
57.740576969	0.26063284735
23.099052811	0.42093485770
9.3882478591	0.24344615121
0 2 3 6.0 1.0	
37.596171210	-0.28991094530E-01
5.1240690810	0.54919083831
2.0119996085	0.93793330488
0 2 1 0.0 1.0	
0.73860686002	1.0
0 3 4 10.0 1.0	
74.129460637	0.14363216676E-01
21.359842587	0.86628177096E-01
7.4995240537	0.25631430541
2.7601394169	0.40374062368
0 3 1 0.0 1.0	
0.95362061236	0.39427042447
0 3 1 0.0 1.0	
0.28420862520	0.23091146816

Zinc

30 12
0 0 8 2.0 1.0

405924.31028	.22442017483E-03
60846.955735	.17402086626E-02
13847.343092	.90513339565E-02
3919.6158551	.36817341445E-01
1276.3594167	.12004850256
458.67254435	.28576057621
178.28725246	.41087462062
70.612192837	.21816962456
0 0 4 2.0 1.0	
443.88077950	-.24934274984E-01
137.55875267	-.11817955766
22.268083479	.55367318468
9.5217310606	.52628934936
0 0 2 2.0 1.0	
14.874114065	-.22929955254
2.4647517612	.71135484742
0 0 1 2.0 1.0	
1.0113272238	1.0
0 0 1 0.0 1.0	
0.40	1.0
0 1 1 0.0 1.0	
0.16	1.0
0 2 6 6.0 1.0	
2205.3508534	.23356240448E-02
522.35300699	.19031022634E-01
167.73055542	.89955758675E-01
62.670045373	.26113248631
25.109749456	.42348448173
10.225142681	.24618926885
0 2 3 6.0 1.0	
40.713442521	-.30029667592E-01
5.6247090696	.55575254864
2.2279949116	.95581013442
0 2 1 0.0 1.0	
0.83354741691	1.0
0 3 4 10.0 1.0	
88.554315311	.12728170015E-01
25.721525557	.79394499843E-01
9.1278367624	.24491506805
3.4312364064	.40390526479
0 3 1 0.0 1.0	
1.2308920645	.40158491145
0 3 1 0.0 1.0	
0.39031845112	.21579805034

References

- [1] Kohn, W.; Sham, L. J. *Phys. Rev.* **1965**, *140*, A1133–A1138.
- [2] Piela, L. *Chasing Correlation Dragon: Density Functional Theory (DFT)*; Elsevier, 2014; pp 663–717.
- [3] Perdew, J. P. Jacob's ladder of density functional approximations for the exchange-correlation energy. AIP Conference Proceedings. 2001.
- [4] Becke, A. D. *J. Chem. Phys.* **2014**, *140*, 18A301.
- [5] Perdew, J. P. *Int. J. Quantum Chem.* **2009**, *28*, 497–523.
- [6] Tao, J.; Perdew, J. P.; Staroverov, V. N.; Scuseria, G. E. *Phys. Rev. Lett.* **2003**, *91*.
- [7] Perdew, J. P.; Ernzerhof, M.; Burke, K. *J. Chem. Phys.* **1996**, *105*, 9982–9985.
- [8] Vogiatzis, K. D.; Polynski, M. V.; Kirkland, J. K.; Townsend, J.; Hashemi, A.; Liu, C.; Pidko, E. A. *Chem. Rev.* **2018**, *119*, 2453–2523.
- [9] Becke, A. D. *J. Chem. Phys.* **1993**, *98*, 5648–5652.
- [10] Vosko, S. H.; Wilk, L.; Nusair, M. *Can. J. Phys.* **1980**, *58*, 1200–1211.
- [11] Lee, C.; Yang, W.; Parr, R. G. *Phys. Rev. B* **1988**, *37*, 785–789.
- [12] Perdew, J. P.; Wang, Y. *Phys. Rev. B* **1992**, *45*, 13244–13249.
- [13] Adamo, C.; Barone, V. *J. Chem. Phys.* **1999**, *110*, 6158–6170.
- [14] Pople, J. A.; Head-Gordon, M.; Fox, D. J.; Raghavachari, K.; Curtiss, L. A. *J. Chem. Phys.* **1989**, *90*, 5622–5629.
- [15] Linnéra, J.; Sansone, G.; Maschio, L.; Karttunen, A. J. *J. Phys. Chem. C* **2018**, *122*, 15180–15189.
- [16] Zhao, Y.; Truhlar, D. G. *Theor. Chem. Acc.* **2007**, *120*, 215–241.
- [17] Heyd, J.; Scuseria, G. E.; Ernzerhof, M. *J. Chem. Phys.* **2003**, *118*, 8207–8215.
- [18] Liu, J. F.; Yin, S.; Wu, H. P.; Zeng, Y. W.; Hu, X. R.; Wang, Y. W.; Lv, G. L.; Jiang, J. Z. *J. Phys. Chem. B* **2006**, *110*, 21588–21592.
- [19] Sawada, H. *Mater. Res. Bull.* **1994**, *29*, 239–245.
- [20] Asbrink, S.; Waskowska, A. *J. Condens. Matter Phys.* **1991**, *3*, 8173–8180.
- [21] Pailhé, N.; Wattiaux, A.; Gaudon, M.; Demourgues, A. *J. Solid State Chem.* **2008**, *181*, 2697–2704.
- [22] Sasaki, S.; Fujino, K.; Takéuchi, Y. *Proceedings of the Japan Academy, Series B* **1979**, *55*, 43–48.
- [23] Robinson, W. R. *Acta crystallogr., B Struct. Crystallogr. Cryst. Chem.* **1975**, *31*, 1153–1160.
- [24] Kirfel, A.; Eichhorn, K. *Acta Crystallogr., Sect. A: Found. Crystallogr.* **1990**, *46*, 271–284.

- [25] Abrahams, S. C.; Bernstein, J. L. *J. Chem. Phys.* **1971**, *55*, 3206–3211.
- [26] Shklover, V.; Haibach, T.; Ried, F.; Nesper, R.; Novák, P. *J. Solid State Chem.* **1996**, *123*, 317–323.
- [27] Kaurova, I. A.; Kuz'micheva, G. M.; Rybakov, V. B. *Crystallogr. Rep.* **2013**, *58*, 226–233.
- [28] Madelung, O. *Semiconductors: Data Handbook*; Springer Berlin Heidelberg, 2004.
- [29] Guha, S.; Peebles, D.; Wieting, T. *J. Phys. Rev. B* **1991**, *43*, 13092–13101.
- [30] Kliche, G.; Popovic, Z. V. *Phys. Rev. B* **1990**, *42*, 10060–10066.
- [31] Sander, T.; Reindl, C. T.; Giar, M.; Eifert, B.; Heinemann, M.; Heiliger, C.; Klar, P. J. *Phys. Rev. B* **2014**, *90*.
- [32] Sanson, A. *Solid State Commun.* **2011**, *151*, 1452–1454.
- [33] Damen, T. C.; Porto, S. P. S.; Tell, B. *Phys. Rev.* **1966**, *142*, 570–574.
- [34] Venger, E. F.; Melnichuk, A. V.; Melnichuk, L. Y.; Pasechnik, Y. A. *Phys. Stat. Sol. B* **1995**, *188*, 823–831.
- [35] Ashkenov, N.; Mbenkum, B. N.; Bundesmann, C.; Riede, V.; Lorenz, M.; Spemann, D.; Kaidashev, E. M.; Kasic, A.; Schubert, M.; Grundmann, M.; Wagner, G.; Neumann, H.; Darakchieva, V.; Arwin, H.; Monemar, B. *J. Appl. Phys.* **2003**, *93*, 126–133.
- [36] Kushwaha, M. S. *Physica B+C* **1982**, *112*, 232–236.
- [37] Wdowik, U. D.; Legut, D. **2009**, *21*, 275402.
- [38] Plendl, J.; Mansur, L.; Mitra, S.; Chang, I. **1969**, *7*, 109–111.
- [39] Sakurai, J.; Buyers, W. J. L.; Cowley, R. A.; Dolling, G. *Phys. Rev.* **1968**, *167*, 510–518.
- [40] Reichardt, W.; Wagner, V.; Kress, W. **1975**, *8*, 3955–3962.
- [41] Merle, P.; Pascual, J.; Camassel, J.; Mathieu, H. *Phys. Rev. B* **1980**, *21*, 1617–1626.
- [42] Guillamet, R.; Lenglet, M.; Adam, F. *Solid State Commun.* **1992**, *81*, 633–637.
- [43] Hayashi, S.; Kanamori, H. *J. Phys. C: Solid State Phys.* **1980**, *13*, 1529–1538.
- [44] Onari, S.; Arai, T.; Kudo, K. *Phys. Rev. B* **1977**, *16*, 1717–1721.
- [45] Kuroda, N.; Fan, H. Y. *Phys. Rev. B* **1977**, *16*, 5003–5008.
- [46] Madelung, O., Rössler, U., Schulz, M., Eds. *Non-Tetrahedrally Bonded Binary Compounds II*; Springer-Verlag, 2000.
- [47] Bhandari, C.; Lambrecht, W. R. L. *Phys. Rev. B* **2014**, *89*.
- [48] Parmigiani, F.; Sangaletti, L. *J. Electron Spectrosc. Relat. Phenom.* **1999**, *98-99*, 287–302.
- [49] Chou, H.; Fan, H. Y. *Phys. Rev. B* **1974**, *10*, 901–910.
- [50] Kurmaev, E. Z.; Wilks, R. G.; Moewes, A.; Finkelstein, L. D.; Shamin, S. N.; Kuneš, J. *Phys. Rev. B* **2008**, *77*.

- [51] Heinemann, M.; Eifert, B.; Heiliger, C. *Phys. Rev. B* **2013**, *87*.
- [52] Marabelli, F.; Parravicini, G. B.; Salghetti-Drioli, F. *Phys. Rev. B* **1995**, *52*, 1433–1436.
- [53] Baumeister, P. W. *Phys. Rev.* **1961**, *121*, 359–362.
- [54] Cheng, C.-S.; Gomi, H.; Sakata, H. *Phys. Status Solid A* **1996**, *155*, 417–425.
- [55] Crawford, J. A.; Vest, R. W. *J. App. Phys.* **1964**, *35*, 2413–2418.
- [56] Marusak, L.; Messier, R.; White, W. B. *J. Phys. Chem. Solids.* **1980**, *41*, 981–984.
- [57] Huffman, D. R.; Wild, R. L.; Shinmei, M. *J. Chem. Phys.* **1969**, *50*, 4092–4094.
- [58] Fujimori, A.; Minami, F. *Phys. Rev. B* **1984**, *30*, 957–971.
- [59] Strehlow, W. H.; Cook, E. L. *J. Phys. Chem. Ref. Data* **1973**, *2*, 163–200.
- [60] Tashtoush, N. M.; Sheiab, A.; Jafar, M.; Momani, S. *Int. J. Phys. Stud. Res.* **2019**, *2*, 59–64.
- [61] Haynes, W. *CRC handbook of chemistry and physics : a ready-reference book of chemical and physical data*; CRC Press: Boca Raton, Florida, 2017.
- [62] Kuklin, M. S.; Karttunen, A. J. **2018**, *122*, 24949–24957.
- [63] Roth, W. L. *Phys. Rev.* **1958**, *110*, 1333–1341.
- [64] Dobin, A. Y.; Duan, W.; Wentzcovitch, R. M. *Phys. Rev. B* **2000**, *62*, 11997–12000.
- [65] Coey, J. M. D.; Sawatzky, G. A. **1971**, *4*, 2386–2407.
- [66] Oguchi, T.; Terakura, K.; Williams, A. R. *Phys. Rev. B* **1983**, *28*, 6443–6452.
- [67] Tenailleau, C.; Suard, E.; Rodriguez-Carvajal, J.; Lacorre, P. *J. Magn. Magn. Mater.* **2004**, *278*, 57–67.
- [68] Goodenough, J. B. *Chem. Mater.* **2013**, *26*, 820–829.
- [69] Linnara, J.; Karttunen, A. J. *Phys. Rev. B* **2019**, *100*.
- [70] Kuz'menko, A. B.; van der Marel, D.; van Bentum, P. J. M.; Tishchenko, E. A.; Presura, C.; Bush, A. A. *Phys. Rev. B* **2001**, *63*.
- [71] Lucovsky, G.; Sladek, R. J.; Allen, J. W. *Phys. Rev. B* **1977**, *16*, 4716–4718.
- [72] Heltemes, E. C.; Swinney, H. L. *J. App. Phys.* **1967**, *38*, 2387–2388.
- [73] Xu, Y.-N.; Ching, W. Y. *Phys. Rev. B* **1993**, *48*, 4335–4351.
- [74] Massidda, S.; Resta, R.; Posternak, M.; Baldereschi, A. *Phys. Rev. B* **1995**, *52*, R16977–R16980.
- [75] Bertoni, C. M.; Cappellini, G.; Finocchi, F.; Monachesi, P. *The surfaces of metal dioxides: TiO_2 and SnO_2* ; Springer Berlin Heidelberg, 2015; pp 404–410.
- [76] Titanium oxide (TiO_2): dielectric constants in rutile: Datasheet from Landolt-Börnstein - Group III Condensed Matter.

- [77] Anthony, J. *Handbook of Mineralogy*; Mineral Data Pub: Tucson, Ariz, 1990; Vol. 3.
- [78] Dhineshbabu, N. R.; Rajendran, V.; Nithyavathy, N.; Vetumperumal, R. *Appl. Nanosci* **2015**, *6*, 933–939.
- [79] Patnaik, P. *Handbook of Inorganic Chemicals*; McGraw-Hill: New York, 2003.
- [80] Abdel-Rahman, M.; Bahidra, E.; Abas, A. F. *Materials* **2020**, *13*, 2002.
- [81] Deer, W. A. *An Introduction to the Rock-Forming Minerals*; The Mineralogical Society: London, 2013.
- [82] Weigend, F.; Ahlrichs, R. *Phys. Chem. Chem. Phys.* **2005**, *7*, 3297.
- [83] Karttunen, A. J.; Tynell, T.; Karppinen, M. *J. Phys. Chem. C* **2015**, *119*, 13105–13114.
- [84] Linnara, J.; Karttunen, A. J. *Phys. Rev. B* **2017**, *96*.
- [85] Glebko, N.; Aleksandrova, I.; Tewari, G. C.; Tripathi, T. S.; Karppinen, M.; Karttunen, A. J. *J. Phys. Chem. C* **2018**, *122*, 26835–26844.
- [86] Pritchard, B. P.; Altarawy, D.; Didier, B.; Gibson, T. D.; Windus, T. L. *J. Chem. Inf. Model.* **2019**, *59*, 4814–4820.
- [87] Oliveira, D. V.; Laun, J.; Peintinger, M. F.; Bredow, T. *J. Comp. Chem.* **2019**, *40*, 2364–2376.